AGU PUBLICATIONS

Geochemistry, Geophysics, Geosystems

RESEARCH ARTICLE
10.1002/2017GC006950

Gravity-Driven Deposits in an Active Margin (Ionian Sea) Over the Last 330,000 Years

Eléonore Köng[1], Sébastien Zaragosi[1], Jean-Luc Schneider[1], Thierry Garlan[2], Patrick Bachèlery[3], Marjolaine Sabine[1], and Laurine San Pedro[4]

[1]EPOC, UMR CNRS 5805, Université de Bordeaux, allée Geoffroy Saint-Hilaire, CS 50023, Pessac, France, [2]SHOM/DOPS/HOM/Sédimentologie, 13 rue du Chatellier, CS 92803, Brest, France, [3]LMV/OPGC, Université Blaise Pascal de Clermont-Ferrand, Campus des Cézeaux, 6 avenue Blaise Pascal, TSA60026 – CS60026, Aubière Cedex, France, [4]Laboratoire Domaines Océaniques, UMR 6538, Université de Bretagne occidentale, IUEM, rue Dumont d'Urville, Plouzané, France

Key Points:
- Turbidite deposits of the Calabrian Arc and the western part of the Mediterranean Ridge over the last 330 ka
- Three gravity-driven deposits' presence/absence phases have been highlighted
- Volcanoclastic deposits could be linked to Etna changing morphology

Supporting Information:
- Supporting Information S1

Correspondence to:
E. Köng,
eleonore.kong@u-bordeaux.fr

Citation:
Köng, E., Zaragosi, S., Schneider, J.-L., Garlan, T., Bachèlery, P., Sabine, M., & San Pedro, L. (2017). Gravity-driven deposits in an active margin (Ionian Sea) over the last 3,30,000 years. *Geochemistry, Geophysics, Geosystems*, *18*, 4186–4210. https://doi.org/10.1002/2017GC006950

Received 4 APR 2017
Accepted 26 OCT 2017
Accepted article online 2 NOV 2017
Published online 29 NOV 2017

Abstract In the Ionian Sea, the subduction of the Nubia plate underneath the Eurasia plate leads to an important sediment remobilization on the Calabrian Arc and the Mediterranean Ridge. These events are often associated with earthquakes and tsunamis. In this study, we analyze gravity-driven deposits in order to establish their recurrence time on the Calabrian Arc and the western Mediterranean Ridge. Four gravity cores collected on ridges and slope basins of accretionary prisms record turbidites, megaturbidites, slumping and micro-faults over the last 330,000 years. These turbidites were dated by correlation with a hemipelagic core with a multi-proxy approach: radiometric dating, δ18O, b* colour curve, sapropels and tephrochronology. The origin of the gravity-driven deposits was studied with a sedimentary approach: grain-size, lithology, thin section, geochemistry of volcanic glass. The results suggest three periods of presence/absence of gravity-driven deposits: a first on the western lobe of the Calabrian Arc between 330,000 and 250,000 years, a second between 120,000 years and present day on the eastern lobe of the Calabrian Arc and over the last 60,000 years on the western lobe, and a third on the Mediterranean Ridge over the last 37,000 years. Return times for gravity-driven deposits are around 1,000 years during the most important record periods. The turbidite activity also highlights the presence of volcaniclastic turbidites that seems to be link to the Etna changing morphology over the last 320,000 years.

1. Introduction

The Ionian Sea, located between Apulia, Calabria and Sicily in Italy and the Ionian Islands and Peloponnese in Greece, is witness to the final stage of closure of Neotethys' southern branch (de Voogd et al., 1992; Faccenna et al., 2001, 2004). The subduction of the Nubia plate underneath the Eurasia plate since the Cretaceous has led to the formation of two accretionary wedges since the Miocene: the Calabrian Arc and the Mediterranean Ridge (Le Pichon & Angelier, 1979; McKenzie, 1978; Minelli & Faccenna, 2010). The formation of these two accretionary wedges over a million years scale (Coy et al., 1983; Dewey & Sengör, 1979; Gallais et al., 2011, 2012; van Dijk & Scheepers, 1995; Truffert, 1992) as well as their morphology and present day functioning have been widely studied (D'Agostino et al., 2008; Gutscher et al., 2016; Huguen et al., 2006; Kreemer & Chamot-Rooke, 2004; Polonia et al., 2011; Tortorici et al., 1995). For the last thousand years, Polonia et al. (2013ab, 2015, 2017) has focused initially on the Holocene's palaeoseismology based on turbidite record and, more recently, studies have been extended to the last 60 ka (Köng et al., 2016). Between these two time scales (million years and the last thousand years) few studies deal with the turbidite record in active margin.

This study try to reconstruct the turbidite activity over a span of hundred thousand years on the wedges in the Ionian Sea. This area have been described as a good place to conduct palaeoseismologic studies for three reasons: (1) the majority of debris flows, turbidites and sliding seem to be distinctive earthquakes-triggered structure (Kastens, 1984; Köng et al., 2016; Polonia et al., 2013aa, 2013ab, 2015, 2016, 2017; San Pedro et al., 2017), (2) sapropels and tephra provide a suitable means of dating events (Kastens, 1984; Löwemark et al., 2006), (3) glacio-eustatism influence is expected to be minor if the area is disconnected from the shelf (Kastens, 1984). This study attempts to decipher which control factor (sea level changes, earthquakes and volcanism) dominates the triggering of gravity-driven sedimentation recorded on ridge

and slope basins of the Calabrian Arc and the Mediterranean Ridge over the last 330,000 years. To achieve these goals, a multiproxy approach was applied to 4 sediment cores that were collected during the MOCOSED2012 oceanographic campaign, aboard RV *Pourquoi Pas?* in 2012.

2. Geological Background

The Calabrian Arc and the Mediterranean Ridge represent 120,000 km^2 (60%) of the Ionian Sea floor (Figure 1). These two accretionary wedges show different orientations. The Calabrian Arc is oriented SW-NE while the western part of the Mediterranean Ridge is oriented NW-SE. They present two growth stages since their inception in the Miocene. The first stage before the Messinian, results in the formation of a first ridge composed by Tertiary and Mesozoic sediments. The second stage after the Messinian, results in the formation of a second ridge with a Messinian evaporites detachment plane at its base surmounted by Plio-Quaternary sediments (Gallais et al., 2012).

2.1. Calabrian Arc

The Calabrian Arc accretionary wedge is located along the eastern Sicilian and Calabrian coasts. In this area the subduction of the Nubia plate underneath the Eurasia plate has been accompanied by the opening of the Tyrrhenian back-arc basin due to the slab retreat over the last 12 Myr (Argnani, 2000; Faccenna et al., 2004), along with the formation of the Aeolian volcanic arc and some isolated volcanoes as Etna or

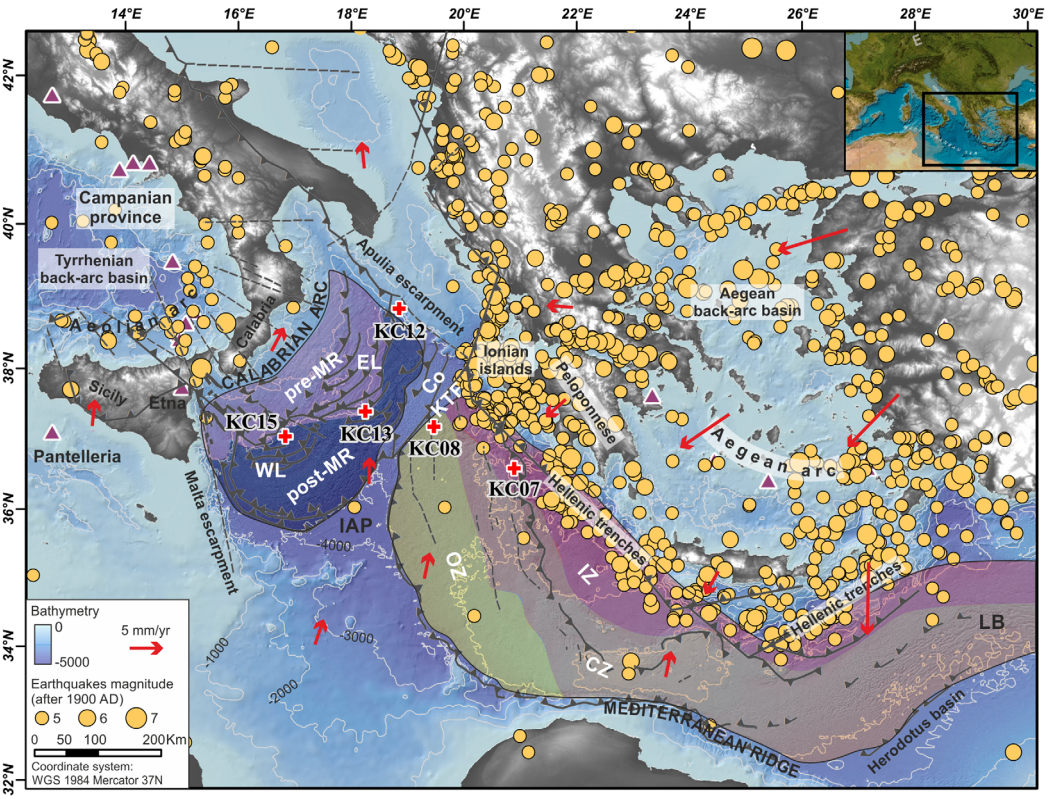

Figure 1. Location map and physiography of the Calabrian Arc and the Mediterranean Ridge. Bathymetry is issued from GEBCO (http://www.gebco.net/) and contours are in meters. The Calabrian Arc structure of the map derived from Polonia et al. (2011). The Mediterranean Ridge structure of the map derived from Huguen et al. (2006). Grey lines and dash lines correspond to tectonic context: faults and overlaps (Gallais et al., 2011; Huguen et al., 2006; Viti et al., 2011). Red crosses show sediment cores used in this study. The purple triangles correspond to volcanoes. Earthquakes data is issue from the USGS (https://earthquake.usgs.gov). Red arrows indicate velocity vectors of plates (Viti et al., 2011). Acronyms correspond to: WL: Calabrian Arc western lobe, EL: Calabrian Arc eastern lobe, pre-MR: pre-messinian ridge, post-MR: post-messinian ridge, IAP: Ionian abyssal plain, Co: corridor between the Calabrian Arc and the Mediterranean Ridge, KTF: Kephalonia Transform Fault, OZ: Mediterranean Ridge outer zone, CZ: Mediterranean Ridge central zone, IZ: Mediterranean Ridge inner zone, LB: Levantine basin.

Pantelleria (Figure 1). The Calabrian Arc extends over 400 km long and 250 km wide. It is bordered by the Malta escarpment to the South-West, the Apulia escarpment to the North-East, and by the Ionian abyssal plain and the Mediterranean ridge to the South-East (Figure 1). The arc is divided into an eastern lobe (EL) and a western lobe (WL) bounded by deformation fronts (Figure 1). Both are separated in two ridges corresponding to the two growth episodes of the wedges: the pre-Messinian ridge, and the post-Messinian ridge linked to the change of basal friction of the wedge induced by the presence of the Messinian evaporites (Polonia et al., 2011).

The recent activity of the subduction is still debated but appears to be locally active at a slow rate of 0.5 mm/yr (D'Agostino et al., 2008; Faccenna et al., 2014; Viti et al., 2011). It is associated with an uplift in Sicily and Calabria, demonstrated by emerged marine terraces. The uplift rate ranging from 0.7 to 1.7 mm/yr since 600 ka in Sicily (Catalano & De Guidi, 2003; Santoro et al., 2013) and is about 1.3 mm/yr in Calabria since the last interglacial period (Dumas et al., 2005). All these studies highlight a slight acceleration of the uplift rates over the last 60 ka. According to the study of Mouslopoulou et al. (2016), the uplift rates appear to be linked with earthquake clustering as suggested for other active margins (Calabria, Makran, Japan, New Zealand, Papaua New Guinea, Greece and Chile).

2.2. Mediterranean Ridge

The Mediterranean Ridge is located south of Greece and Crete from the Ionian Sea to the Levantine basin (Figure 1). It extends over 1,500 km long and 200–250 km wide (Emery et al., 1966). In this area, the subduction rate is 3 cm/yr (Dewey & Sengör, 1979; Kreemer & Chamot-Rooke, 2004; Le Pichon et al., 1995; McClusky et al., 2000; Olivet et al., 1982; Reilinger et al., 1997). The subduction is accompanied by the formation of the Aegean back-arc basin and the Aegean volcanic arc (Figure 1). This accretionary wedge is bordered to the north by a series of deep troughs (the Hellenic trenches) ranging from 3,000 to 5,000 m in depth, the Ionian abyssal plain to the west, to the south by the Libyan continental shelf and the Herodotus basin to the east (Figure 1). It is composed of three different morphological domains (from west to east): an outer folded zone, a central relatively flat area and an inner plateau extending to the south of the deep troughs (Truffert, 1992).

The western part of the Mediterranean ridge, located in the Ionian Sea, is not only the deepest part ($>$ 3,000 m) but also the widest part ($>$ 250 km) (Huguen et al., 2006; Reston et al., 2002). The north-west termination of the Mediterranean ridge is bounded by the Calabrian Arc and the Kephalonia Transform Fault (Figure 1: KTF). The transition between the Calabrian Arc and the Mediterranean Ridge is marked by a corridor composed by NE-SW ridges to the north of the KTF (Huguen et al., 2006).

The active subduction leads to an uplift highlighted by emerged marine terraces in Greece. In the Peloponnese, the uplift ranges from 0.3 to 0.8 mm/yr for the last 250 ka (Fountoulis et al., 2014) and from 0.1 to 0.3 mm/yr in the Ionian islands during the last 400 ka (Zelilidis et al., 1998).

3. Sedimentological Background

3.1. Co-Seismic Sedimentation

In marine environments strongly influenced by seismicity, earthquakes can be recorded in sediment deposits by several specific types of depositional structures. The main three are described below:

1. Liquefaction is linked to an increase of the pore-water pressure in sediments (Owen, 1987). It results in formation of folds, convolute bedding and fluidization. Sedimentary deposits then formed "mixed layers" defined by folded layers enclosed between undeformed beds (Marco & Agnon, 1995; Rodríguez-Pascua et al., 2000). Liquefaction can evolve to slumping when sediments are moved laterally.
2. Microfracturation is visible in more indurated sediments. Ductile sediments show loop bedding (Calvo et al., 1998) that can evolve into faults when lithification and deformation increase (Calvo et al., 1998).
3. In some cases, as described by Heezen and Ewing (1952) for the first time about the 1929 earthquakes in Grand Banks of Newfoundland, earthquakes can generate sediment destabilizations or sliding that can evolve to turbidity currents. Several studies have led to the development of a paleoseismicity approach based on marine sediments records (Goldfinger et al., 2003, 2012; Gutiérrez-Pastor et al., 2013; Huh et al., 2004; Pouderoux et al., 2012, 2014; Völker et al., 2011). This approach have been widely used in Mediterranean area (Anastasakis & Piper, 1991; Kastens, 1984; Köng et al., 2016; Polonia et al., 2013aa, 2013ab,

2015, 2016; San Pedro et al., 2017). Nevertheless, it is not always easy to link a sedimentary deposit to a particular earthquake. Several clues are necessary (Goldfinger, 2011): turbidites deposits must spread a large geographical expansion; the sedimentary deposits composition is usually diversified or presents sedimentological figures as convolutes (Rodríguez-Pascua et al., 2000) or amalgamated bed (Goldfinger et al., 2008; Gutiérrez-Pastor et al., 2013; Hassoun et al., 2014; Migeon et al., 2017; Nakajima & Kanai, 2000; Nelson et al., 2012; Noda et al., 2008; Patton et al., 2015). In confined basins, a « seiche effect » can affect water masses and generate the deposition of homogenites (Chapron et al., 1999; Maria Bianca Cita et al., 1996; Kastens & Cita, 1981).

In the Ionian Sea, possible co-seismic sedimentation has been studied especially through homogenites and turbidites deposits. Homogenites have been described for the first time by Kastens and Cita (1981). They can be related either to co-seismic events associated with the propagation of tsunami waves (Cita & Aloisi, 1999; Polonia et al., 2013a), or to low sea level periods associated with destabilization of the continental shelf or gas hydrates as described by Reeder et al. (2000) and Rothwell et al. (2000) in the Levantine basin and the occidental Mediterranean basin. On the Calabrian Arc and the Ionian abyssal plain, turbidite activity has been linked to seismic and/or tsunamis by Kastens (1984), Polonia et al. (2013aa, 2013ab, 2015, 2016), San Pedro et al. (2017) for the Holocene and more recently for the last 60 ka by Köng et al. (2016).

3.2. Volcanism and Tephra Deposits

The subduction system in the Ionian area, as described previously, is accompanied by the formation of Tyrrhenian and Aegean back-arc basins, and active volcanic arcs, the Aeolian and Aegean Islands, and by volcanic provinces. The Plio-Quaternary Italian volcanism can be separated into nine different provinces (Peccerillo, 2005): Tuscany, intra-Apennine, Roman, Ernici-Roccamonfina, Campanian, Aeolian Arc, Sicily, Sardinia and Southern Tyrrhenian Sea. The three most frequently active volcanic provinces as described by Peccerillo (2005) are:

1. the Campanian province has been active for 1 Myr. Potassic to ultrapotassic compositions and sometimes calc-alkaline compositions characterized the Campanian volcanism.
2. The Aeolian Arc province has been active for 1 or 0,4 Myr. Mafic and intermediate and minor silicic rocks characterize it. The central islands are dominated by calc-alkaline to shoshonitic mafic to silicic rocks. The eastern arc is dominated by calc-alkaline to potassic alkaline rocks.
3. The Sicily province has been active for 7 Myr. It is characterized by rocks of mafic to intermediate composition and pre-alkaline rhyolites at Pantelleria. The main volcanoes are Etna (0.5 Ma to present) and Pantelleria (0.3 Ma to 0.005 Ma). Currently, Etna is a stratovolcano but its morphology and magmatism has changed during the last 500,000 years. It started as submarine volcanism, emerged 320,000 years ago as a subaerial fissure-type, evolved to a shield volcano around 220,000 years ago, then to a polygenic central-volcano around 120,000 years ago, and to the present day stratovolcano around 60,000 years ago (Branca et al., 2008; Kieffer, 1985).

Wind circulations from West to East, called westerlies, favor the emplacement of tephra layer's deposition from Italian volcanoes in the Ionian Sea (Insinga et al., 2014). Aegean arc products, however, are primarily dispersed in the eastern part of the Mediterranean Sea such as the Levantine basin (Çağatay et al., 2015; Hamann et al., 2010; Wagner et al., 2008).

The study of Insinga et al. (2014) has led to synthesis of the volcanic events recorded in the Ionian basin over the last 200 kyrs. The main marked layers recorded in the entire basin are deposits from the Phlegrean Fields Y5 and X6 respectively dated by geochronology $^{40}Ar/^{39}Ara$ at 39.28 $\pm$ 0.11 ka BP (De Vivo et al., 2001) and 108.9 $\pm$ 1.8 ka BP (Iorio et al., 2014) and Y1 deposit from Etna volcano dated by $\delta^{18}O$ at 16.7 ka BP (Albert et al., 2013; Insinga et al., 2014; Keller et al., 1978).

3.3. Sapropels

The Mediterranean Sea sediments are punctuated by the presence of dark sediments layers. These deposits, called sapropels, are characterized by the presence of organic matters and the absence of benthic fauna. They reflect the occurrence of a large deep marine anoxia. These anoxia events can be explained by an increase of biological sea surface productivity (Boyle & Lea, 1989; Calvert, 1983; Calvert et al., 1992; De Lange & Ten Haven, 1983; Pedersen & Calvert, 1990; Van Os et al., 1994) and/or by a decrease of the deep

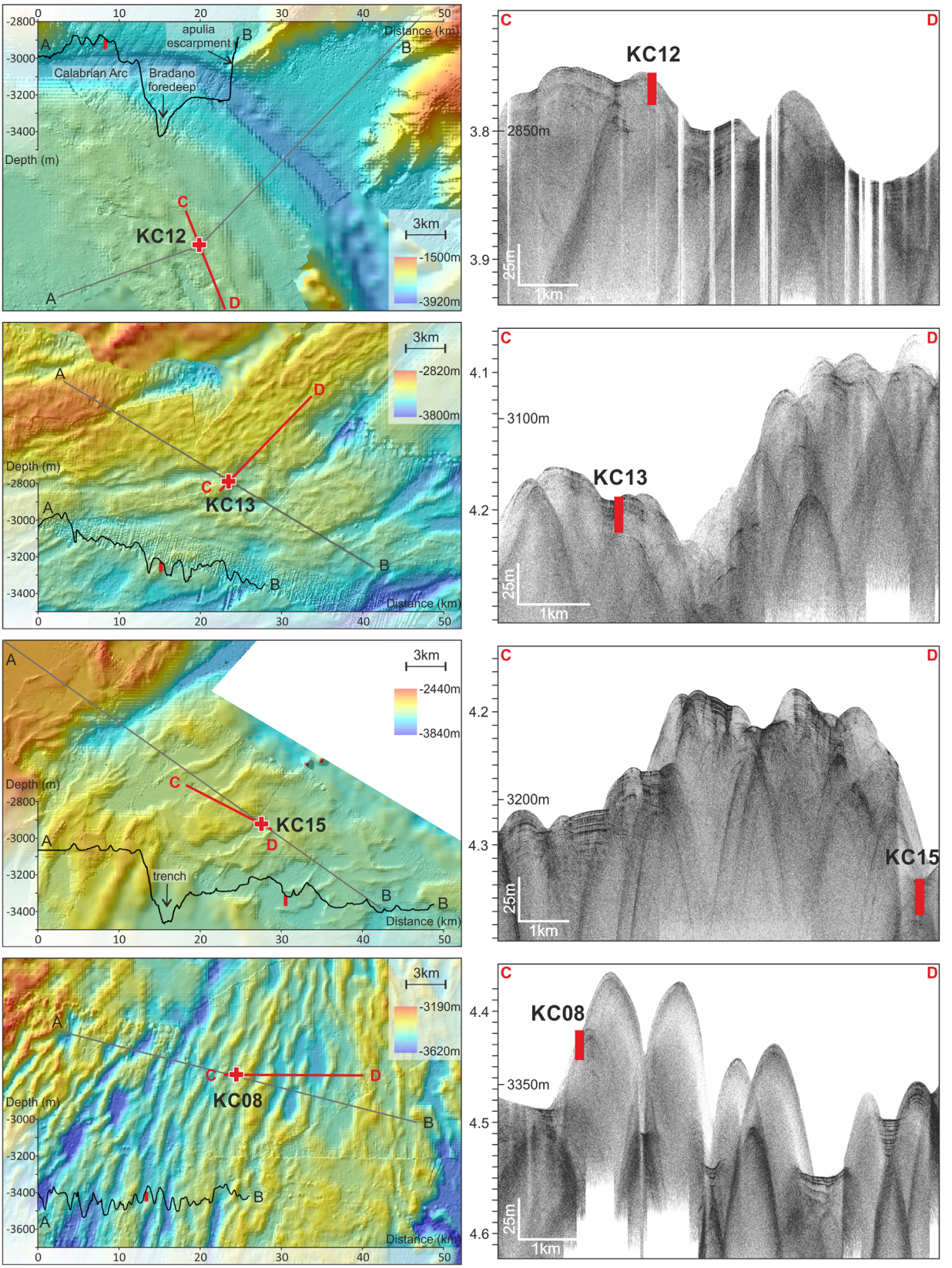

Figure 2. Close-up on the cores locations. Bathymetry is issued from MOCOSED2012 cruise. Longitudinal depth profiles are at the same scale and present the local morphology. CHIRP profiles from MOCOSED2012 cruise present stratigraphy of the core's locations areas, their locations are represented with a red line on bathymetry.

ventilation (Cita & Grignani, 1982; Cita et al., 1977; Olausson, 1961; Rohling, 1994; Ryan, 1972; Thunell et al., 1977; Vergnaud-Grazzini, 1985; Vergnaud-Grazzini et al., 1977). Eleven sapropel layers have been recognized over the last 330 kyrs in the Ionian Sea (Emeis et al., 2004; Lourens, 2004).

4. Methods

4.1. Acoustic Imaging

The bathymetric metadata and Digital Terrain Model data products have been derived from the EMODnet Bathymetry portal (www.emodnet-bathymetry.eu).

High-resolution multibeam bathymetry and sub-bottom seismic lines data were collected on the coring sites during the SHOM (French Hydrographic and Oceanographic Marine Service) oceanographic campaign MOCOSED2012 on RV *Pourquoi Pas?* using respectively a multibeam echosounder Reson 7150 (12 kHz) with a spatial resolution of 40 m and chirp sonar Echoes 3500 emitting chirp pulses with a frequency modulation varying from 1.7 to 5.3 kHz (Figure 2).

4.2. Sediment Core Analysis

4.2.1. Piston Cores

Piston cores were collected during the oceanographic campaign MOCOSED2012 with a 4 tons Calypso corer. Table 1 summarizes core collection information. The visual description has been performed on board in order to characterized the quality of the cores, the main lithologies and distinguish the sedimentary facies.

4.2.2. X-ray Imagery

Thin slabs (15 mm thick) were sampled and analyzed with the SCOPIX X-ray image processing tool (Migeon et al., 1999). X-rays allow the distinction between various densities with grey levels in order to highlight sedimentary structures.

4.2.3. Grain Size

The cores were sampled with a step varying from 1 to 50 mm, depending on changes in sedimentological structures. Sediment was analyzed using two Laser Diffraction Malvern^{TM} Granulometers (MASTERSIZER S and MASTERSIZER 2000G) at the EPOC laboratory (University of Bordeaux). The first mode(AQ: Please note that "1st Mode" and "1st mode" has been changed to "first mode" throughout the text for consistency. Kindly confirm.) of the grain-size distribution was calculated with GRADISTAT v8 (Blott & Pye, 2001). Grain size highlights coarser sedimentary structures and allows layers to be linked with a depositional mechanism such as turbidity currents for example.

4.2.4. Petrographic Observations

Petrographic observations were performed with a Leica DM6000 B Digital Microscope on thin sections of remarkable sequences. Thin sections were obtained from fresh cores after induration with a resin (Zaragosi et al., 2006), which allows the high-resolution observation of preserved sedimentary structures.

4.2.5. Organic Carbon Content

The *organic carbon content* was determined on dry weight sediment by combustion in a LECO CS 125 analyzer at the EPOC laboratory (University of Bordeaux). Samples were acidified in crucibles with 2N HCl to destroy carbonates, and then dried at 60°C to remove inorganic carbon and most of the remaining acid and water. The analyses were performed by direct combustion in an induction furnace, and the CO_2 formed was determined quantitatively by infrared absorption.

4.2.6. Geochemical Data

Geochemical data were acquired on a cm-scale with an AVAATECH^{TM} XRF core-scanner at the EPOC laboratory (University of Bordeaux) using the 10 and 30 kV instrumental settings. Sulphur content highlights the sapropel layers when the value is high due to the affinity of sulphur with organic matter (Warning & Brumsack, 2000).

Table 1
Cores' Locations in Degrees, Cores' Length, and Depths Sampling

Core	Longitude (E)	Latitude (N)	Water depth (m)	Cores' lenght (m)
KC07	36.5598	20.8781	3,410	10.50
KC08	37.1016	19.3741	3,438	10.43
KC12	38.6600	18.7933	2,888	10.93
KC13	37.3072	18.2314	3,215	10.35
KC15	36.9429	16.9019	3,326	18.08

4.3. Stratigraphy

4.3.1. AMS Dating

AMS dating was performed at the "Laboratoire de Mesure du Carbone 14" in Saclay (SacA) through the "ARTEMIS" radiocarbon age dating program. Analyses were performed on planktonic foraminifera

collected in the hemipelagic facies, *Globigerinoides ruber* when sufficient material was available, and on *Globigerinoides bulloides* when there was not. ^{14}C radiometric dates are calibrated by MARINE13 curve with a global ocean reservoir of 400 years (Reimer et al., 2013; Siani et al., 2001).

4.3.2. $\delta^{18}O$

$\delta^{18}O$ was measured at the EPOC laboratory (University of Bordeaux) by an Optima mass spectrometer on planktonic foraminifera. In the Mediterranean Sea the presence of sapropels does not allow the analysis on benthic foraminifera (Emeis et al., 2003; Löwemark et al., 2006; Negri et al., 1999). Measurements were performed at a 10 cm interval on *Globigerinoïdes ruber* and *Globigerina bulloïdes* when *G. ruber* was absent. Core KC07 located on the Mediterranean Ridge, on the edge of the Calypso trench, was chosen as a reference for the dating as it records exclusively hemipelagic sediments.

Cores used in this study were correlated with core KC07 with a color index. Lab color space corresponds to the CIELAB system (Debret et al., 2011). It is visualized as a spherical coordinate system with three axes: lightness (L) ranging from 0% to 100%, and chromaticity variables a* and b*. Variable a* corresponds to green (low values) to red (high values) and b* corresponds to blue (low values) to yellow (high values). Lab color space was measured with a Minolta spectrocolorimeter at a 3 cm step. In cores from the Ionian Sea, the colour of sediments alternate between orange, blue and dark brown. Therefore, the colour component used in this study is b*. Correlations were performed manually with the Analyseries software (Paillard et al., 1996). $\delta^{18}O$ measures were performed in addition on the core KC15 because of the important disruption of b* signal due to the presence of turbidites layers.

4.3.3. Sapropels

They are used as "marked horizon" for correlation between the cores because they are widely studied and precisely dated in the Mediterranean Sea (e.g., Emeis et al., 2003, 2004; Löwemark et al., 2006; Thunell et al., 1977).

4.3.4. Tephrochronology

Tephra deposits were recognized in cores visually, by their low density on X-ray imagery. Volcanic glasses were collected in tephra deposits and analyzed on the coarse glasses with a WDS electron microprobe CAMECA SX100 at the University of Clermont-Ferrand (Laboratoire Magma et Volcans - LMV). An accelerating voltage of 15 kV, a 8-nA-beam current with a beam diameter of 20 μm to reduce Na loss were used. The beam current was reduced to 4 nA and the beam diameter to 10 μm when grains were too small for the 20 μm beam. The counting time was 10 s for Na, Ca, Ti, P and Si; 20 s for Mg and Al; 30 s for Mn and 40 s for Fe and K. The detailed procedure is described in Óladóttir et al. (2011). Geochemistry of major oxides, SiO_2 and alkaline sum ($Na_2O + K_2O$), allow classification of volcanic glasses in accordance with Le Bas et al. (1986) lava classification.

5. Results

5.1. Core Location Settings

Core KC12 (Table 1), 1,093 cm long, was collected in the edge of the north-eastern part of the Calabrian Arc (Figures 1 and 2). The core is located 500 m above the base of the Bradano foredeep enclosed between the Calabrian Arc and the Apulia escarpment.

Core KC13 (Table 1), 1,035 cm long, was collected in an accretionary ridge in the eastern part of the Calabrian Arc (Figures 1 and 2). This accretionary ridge is 80 m high and separates two small 2 km^2 slope basins.

Core KC15 (Table 1), 1,808 cm long, was collected in a 2 km^2 slope basin of the south-western part of the Calabrian Arc (Figures 1 and 2). This slope basin is elongated and enclosed between two accretionary ridges of respectively 60 and 50 m height from the base of the basin.

Core KC08 (Table 1), 1,043 cm long, was collected on the slope of an accretionary ridge on the north-western part of the Mediterranean ridge (Figures 1 and 2). The ridge is 90 m high from the base of the basins around.

Core KC07 (Table 1), 1,046 cm long, was collected on the inner zone of the Mediterranean Ridge, on the edge of the Calypso trench (Figures 1 and 3). This core is exclusively used as a reference for stratigraphy.

5.2. Sedimentary Facies and Structures

Eight sedimentary facies were identified in all cores, on the basis of grain size, lithological analysis, X-ray imagery and thin-section analysis.

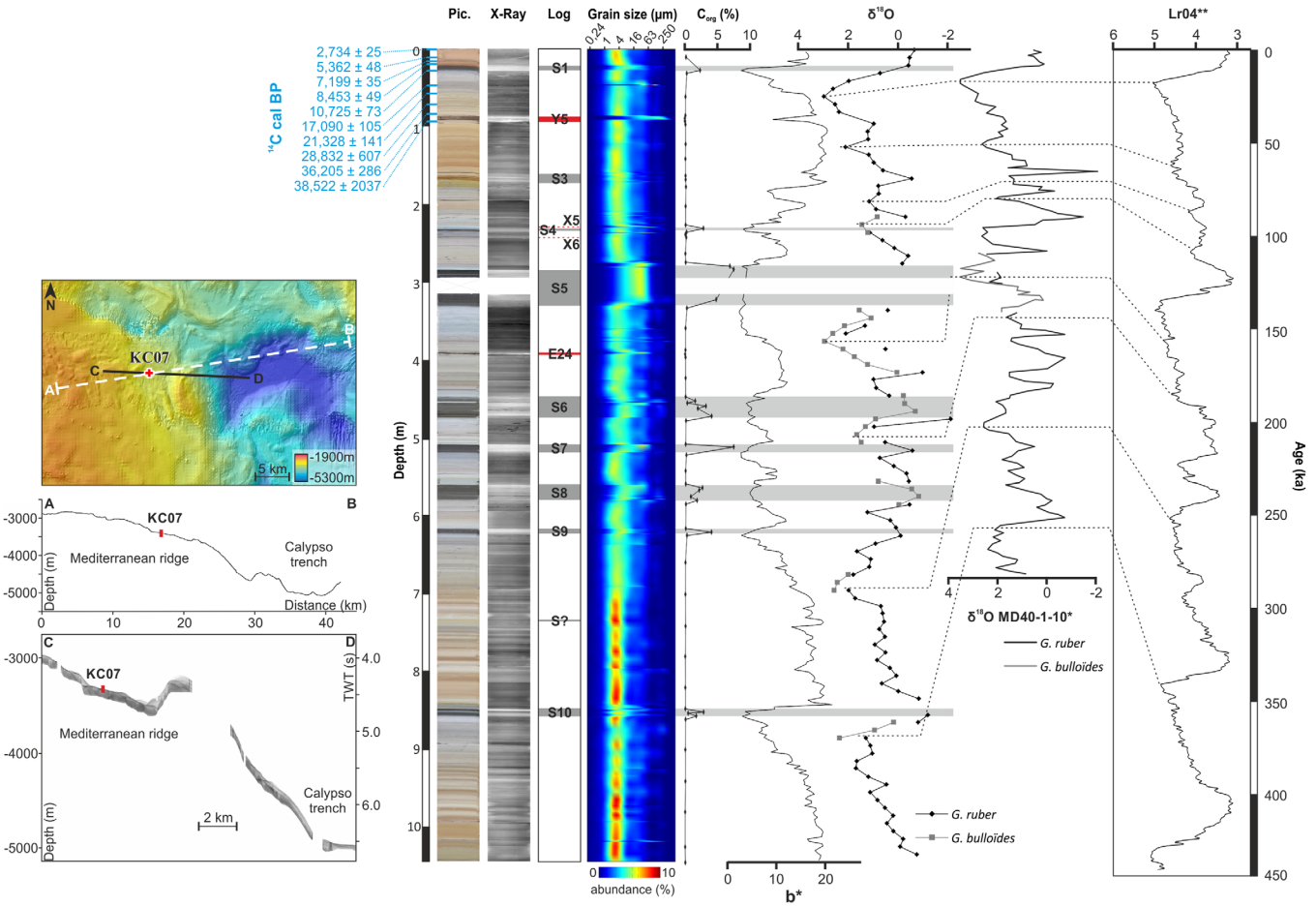

Figure 3. Close-up on the KC07 core location. Core KC07 dating. Radiometric dating (in blue), photograph, X-ray, Log, grain size, b* curve, Sulfur content, Organic carbon content, $\delta^{18}O$ curve and correlation with $*\delta^{18}O$ curve of MD40-1-10 from Löwemark et al. (2006) and $\delta^{18}O$ curve LR04 from Lisiecki and Raymo (2005). Bathymetry is issued from MOCOSED2012 cruise. Longitudinal depth profiles are at the same scale and present the local morphology. CHIRP profiles from MOCOSED2012 cruise present stratigraphy of the core's locations areas, their locations are represented with a black line on bathymetry.

5.2.1. Hemipelagic (Hp) (Figure 4: in White)

Hemipelagic intervals consist of blue/green to brown, fine-grained (3 < first mode < 4 μm), clay layers with planktonic foraminifera fossils and occasionally bioturbations. This facies appears pale grey colored (low density) under X-ray imagery.

5.2.2. Sapropel (Figure 4: in Grey)

Sapropels layers are characterized by a dark brown to grey colored clay (6 < first mode < 8 μm) with a sharp contact at the base and the top with the hemipelagic facies. This facies appears strongly light colored (low density) under X-ray imagery because of its composition of 2–7% of marine organic matter (Figure 3), and abundant foraminifera and pteropods. They are also characterized by a high Sulphur and Barium content and by low values of the b* color index in the most cases. However, they can also be highlighted by high b* and Manganese values when they have been re-oxidized.

5.2.3. Turbidite (Figure 4: in Black, and Figure 5)

This type of deposit is characterized by a sharp to erosive contact, the base ranges from a grey very fine sand layer to medium silts (15 < first mode < 60 μm) which are generally massive. The whole bed is graded upward and evolves into a homogeneous greenish clay sequence (4 < first mode < 5 μm) that corresponds to the decantation of the turbidite plume. This facies appears dark colored (high density) at the basis and evolved into medium grey coloration to the top under X-ray imagery. The base of this sequence shows amalgamated coarser beds with planar laminations and is mainly composed of biotite, muscovite and minor quartz.

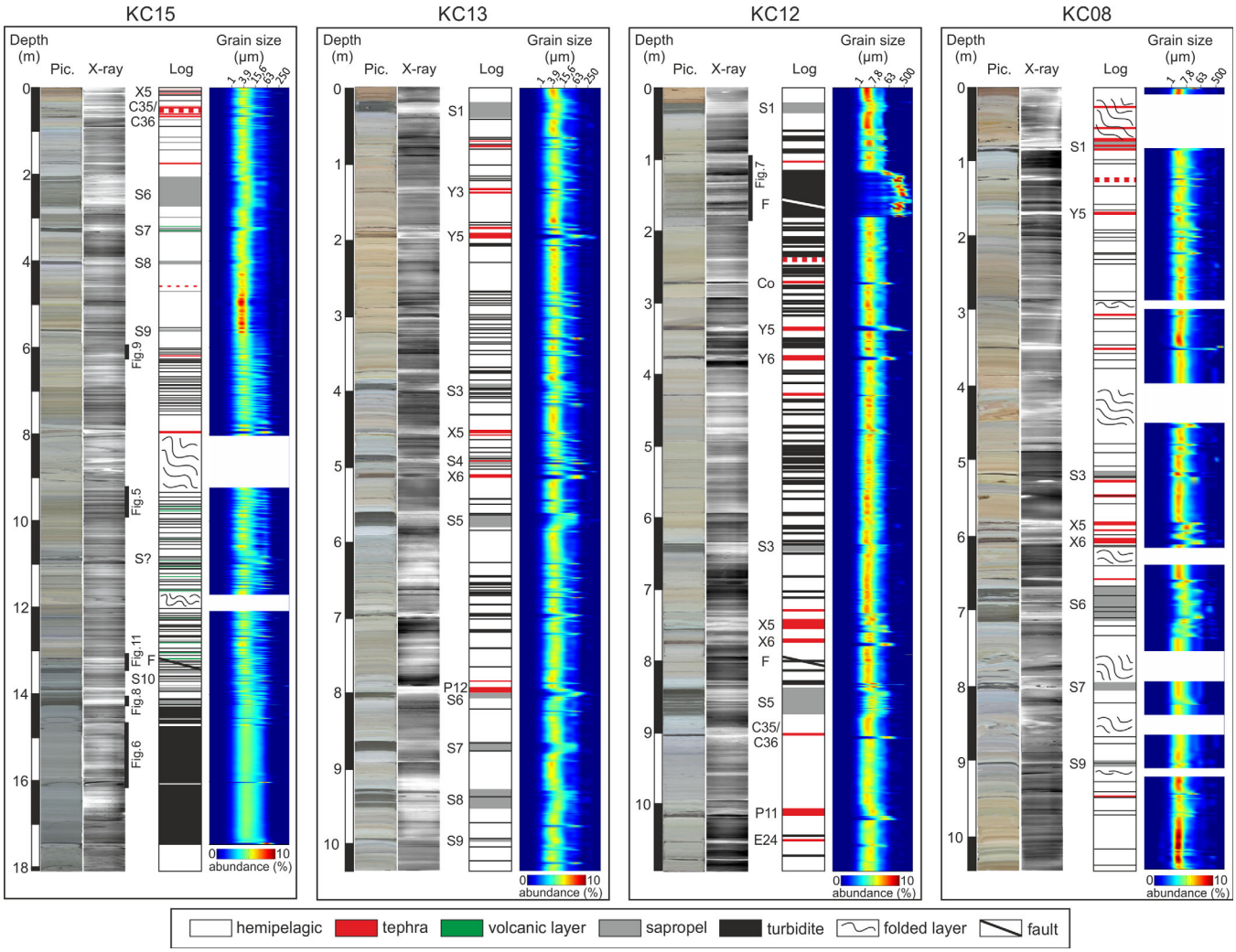

Figure 4. Sedimentary logs and facies occurrence. Core's locations are presented on Figure 1. Grain size distribution is represented by cartography of the relative abundance of each fraction in percent (from dark blue for low abundance to dark red color for high abundance).

5.2.4. Megaturbidite (Figure 4: in Black, and Figure 6)

The deposits of this facies are similar to the turbidite facies but it is thicker (pluridecimetric to metric) compared to the other turbidites of the same area. It can be divided in two sub-groups: silty and sandy megaturbidite. The silty megaturbidites present a sharp to erosive contact, the base ranges from very fine sand to medium silt layers, which are generally massive ($15 <$ first mode < 100 μm). The deposit is graded upward and eventually evolves into a homogeneous clay sequence ($4 <$ first mode < 5 μm). The basis of these sequences shows millimetric amalgamated coarser beds with planar laminations, convolutes and is mainly composed of biotite, muscovite, quartz and some planktonic foraminifera. Two silty megaturbidites are present in core KC15. Only one sandy megaturbidite has been observed in core KC12 (Figure. 7). It is characterized by a sharp to erosive contact, the base is very massive, highly laminated and the granularity ranges from very coarse to fine sand ($200 <$ first mode < 900 μm). It is composed by an alternation of quartz rich laminations (quartz, planktonic and benthic foraminifera) and carbonate rich lamination (planktonic and benthic foraminifera, corals, shell fragment and volcanic glass). The deposit rapidly graded upward from medium silt to clay. That part in mainly composed by quartz, planktonic foraminifera and mica.

5.2.5. Tephra (Figure 4: in Red)

Tephra layers present a progressive base and top, and are composed of volcanic glasses with a homogenous chemical composition (trachytic to phonolitic, depending on the source) and minerals (pyroxene, amphibole, alkali feldspar).

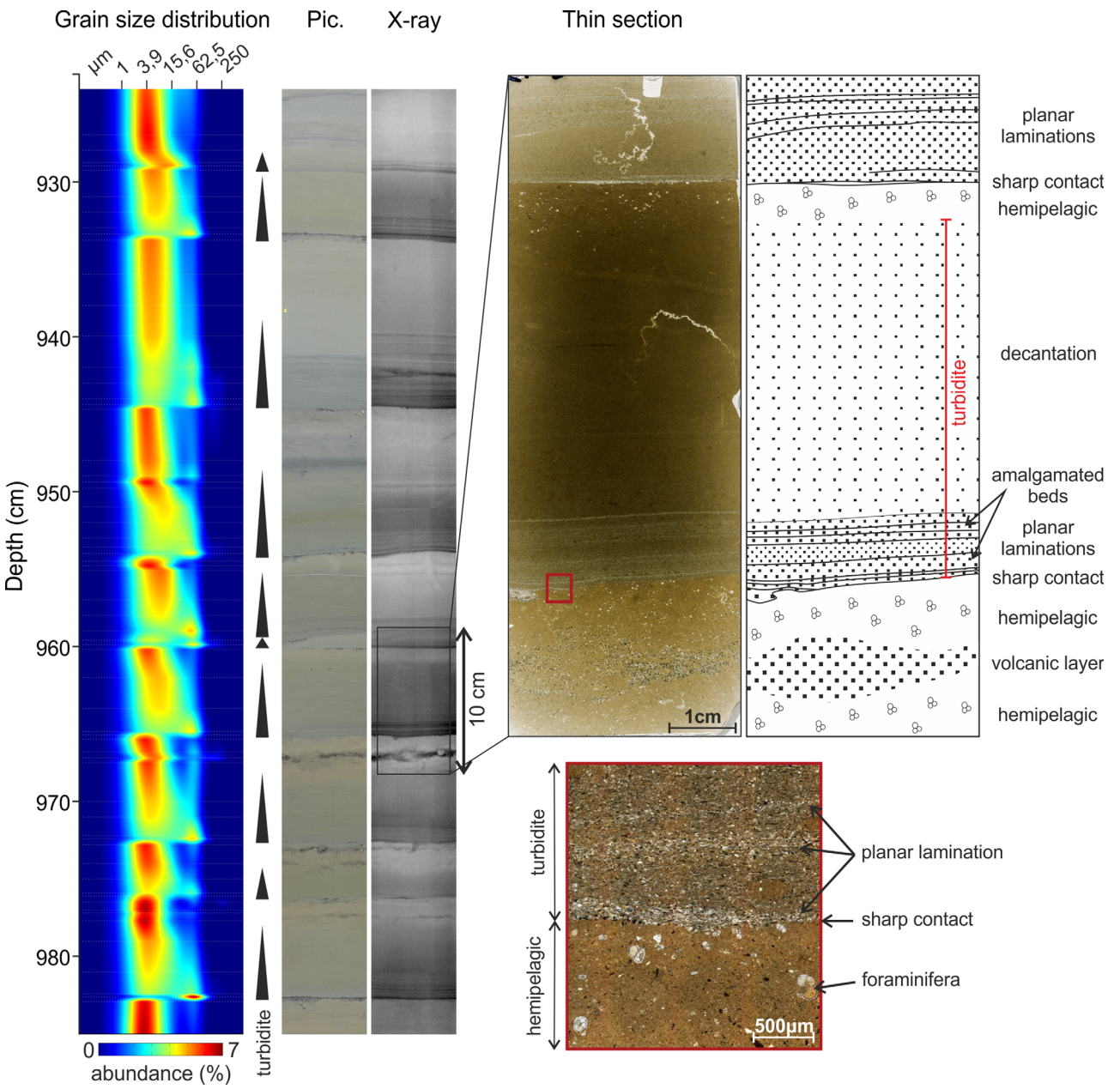

Figure 5. Grain size measurements, X-ray pictures and thin section of the turbidite facies present in core KC15. Grain size distribution is presented by cartography of the relative abundance of each fraction in percent (from dark blue for low abundance to dark red color for high abundance). Core location in Figure 1.

5.2.6. Volcaniclastic Layers (Figure 4: in Green and Figure 8)

Volcanic layers are only present in core KC15. These layers are centimetre thick and characterized by a first mode of grain size around 30 μm. They are composed of volcanic glasses, scoria and minerals (pyroxene, amphibole, alkali feldspar). The analysis of one layer revealed a trachytic composition similar to the Etna magmatism. The difference between this facies and the tephra facies is that volcaniclastic layers correspond to remobilized volcanic material instead of tephra which corresponds to primary deposits and are concomitant to a volcanic eruption.

5.2.7. Folds and Liquefaction (Figures 4, 9, and 10)

These structures are visible due to the undulation formed by old sedimentological structures (e.g., as turbidites) enclosed between undeformed beds. It corresponds to the disturbance of pre-existing deposits due to liquefaction or to a sliding. Bases are non-erosive and surmounted by anisopachous and lenticular folds, and most homogenous layers at the top.

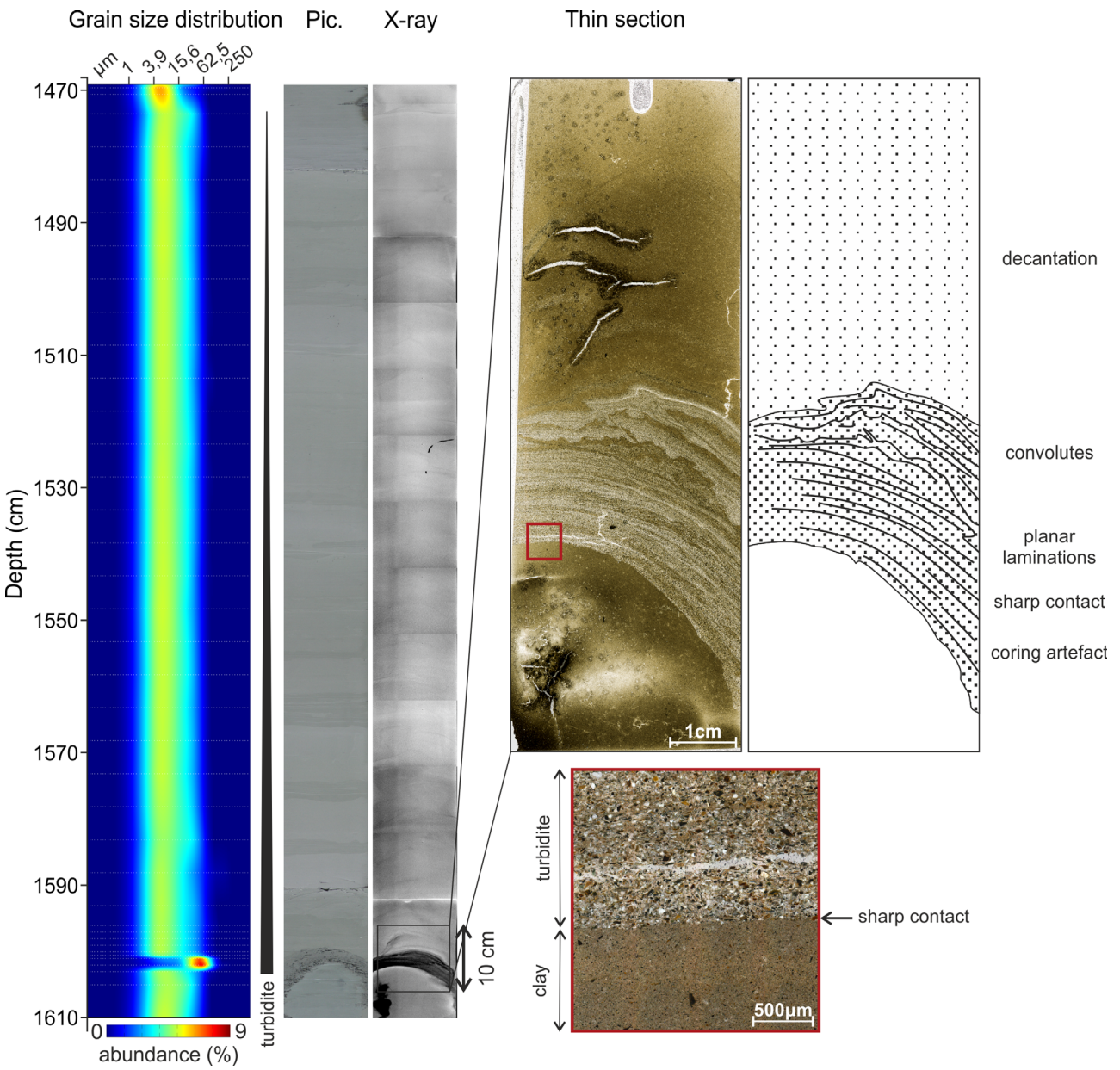

Figure 6. Grain size measurements, X-ray pictures and thin section of the megaturbidite facies present in core KC15. Grain size distribution is presented by cartography of the relative abundance of each fraction in percent (from dark blue for low abundance to dark red color for high abundance). Core location in Figure 1.

5.2.8. Faults (Figures 4 and 11)

These structures are visible due to a vertical gap which affects pre-existent sedimentological structures. The faults recognized in this study are normal and have a millimetre to centimetre vertical throw.

5.3. Stratigraphy

5.3.1. Age Model for Core KC07

The age model of core KC07 were performed by an R software package Clam 2.2 (Blaauw, 2010) with a linear interpolation method and 1 cm resolution. On the first meter of core KC07 it is based on ten radiometric dating performed (Table 2 and Figure 3). They provide ages ranging from 2,734 $\pm$ 25 years to 38,522 $\pm$ 2037 years with no age inversions. On the next 9 meters of the core, δ^{18}O curve (Figure 3) was compared to curves obtained on cores M40/1–10 by Löwemark et al. (2006) in the Ionian Sea and the Levantine basin and to the LR04 δ^{18}O stack provides by Lisiecki and Raymo (2005). The sedimentary record of KC07 extends

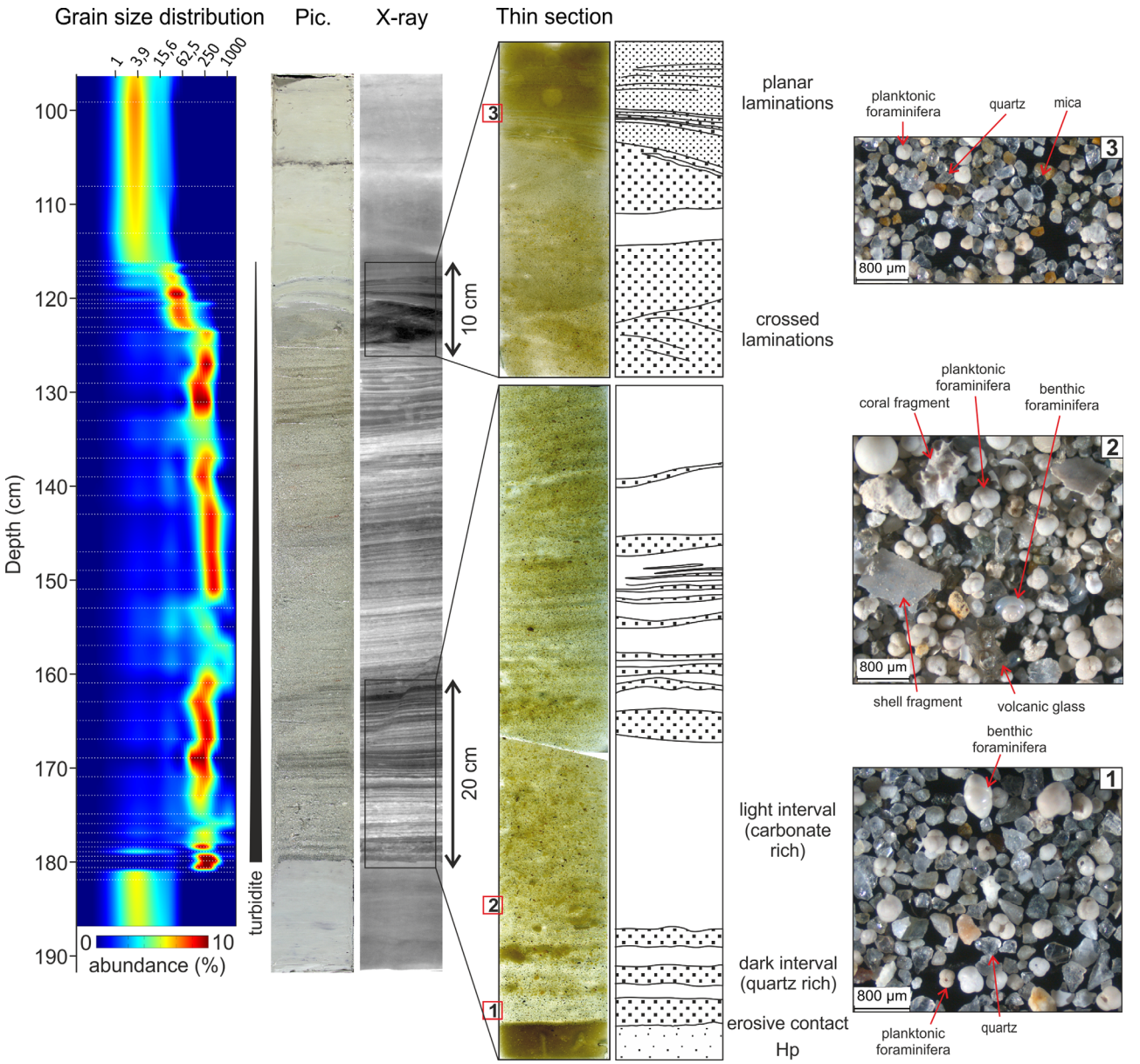

Figure 7. Grain size measurements, X-ray pictures, thin section and grains photography of the megaturbidite facies present in core KC12. Grain size distribution is presented by cartography of the relative abundance of each fraction in percent (from dark blue for low abundance to dark red color for high abundance). Core location in Figure 1.

to the last 400 kyrs and therefore covers the last 4 climatic cycles, from MIS11 to MIS1. KC07 age model is presented in Figure 3. Sapropels bases ages from Emeis et al. (2003) and tephra have been added on the age model curve, but they are not taken into account for the calculation, in order to strengthen results obtained with $\delta\,^{18}O$ only.

5.3.2. Correlations Between the Cores

The correlation between the cores KC12, KC13, KC15 and KC08 with KC07 was performed manually using the b* curve. $\delta^{18}O$ measurements show values ranging from -2 and 3.7 ‰ (Figure 3). Hot isotopic stages show values ranging from -2 and 1 ‰ while cold isotopic stages present values ranging from 1 and 3.7 ‰, with the exception of isotopic stage 6 that shows values lower than 1 in the first half of the stage. The b* curve highlights four periods (Figure 12): three correspond to isotopic stage 11-10, 9-8 and 4-3-2 where sediment is orange and changed to blue, one is dominated by blue sediment during isotopic stages 7 to 5. These periods are common to all the cores of the Ionian Sea and allow good correlation between one and

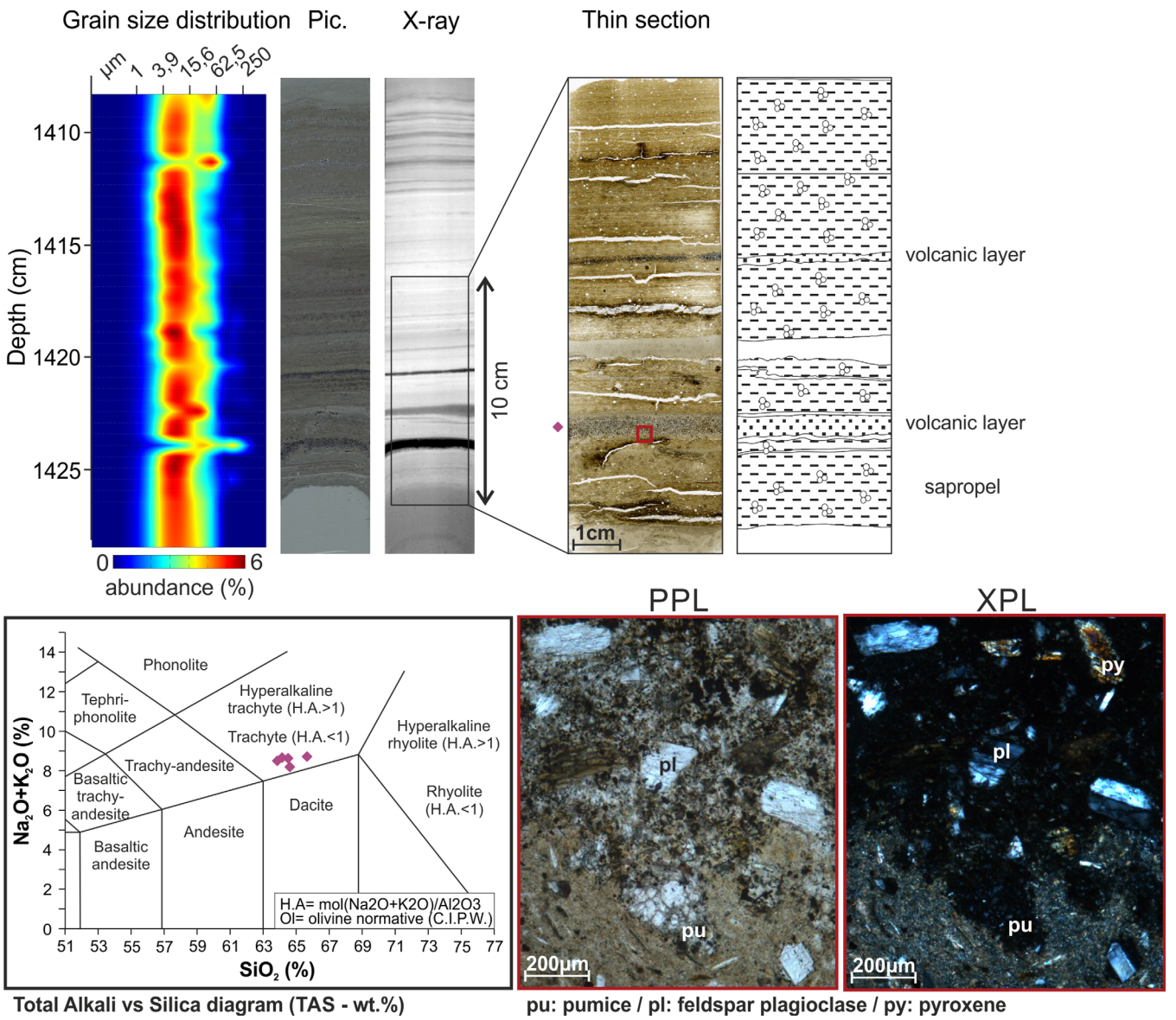

Figure 8. Grain size measurements, X-ray pictures, thin section and Total Alkali versus Silica (TAS – wt. %) diagram (Le Bas et al., 1986) of the volcanic layer facies present in core KC15. Grain size distribution is presented by cartography of the relative abundance of each fraction in percent (from dark blue for low abundance to dark red color for high abundance). PPL corresponds to plane polarized light and XPL to crossed polarized light. Core location in Figure 1.

other (Löwemark et al., 2006; Murat, 1984). Sapropels and tephra are used in order to enhance correlations as marked layers. Therefore, they were not used in order to establish the age model and the dating obtained by correlation with core KC07 were compared with those of the literature.

5.3.3. Time Marker

KC07 core ranges from present time to 400 ka (Figure 12). Sapropels S1 to S10 are observed and one tephra layer has been identified (Figures 12 and 13; Table 3).

KC12 core ages range from present time to 160 ka (Figure 12). Sapropels S1 to S5 are observed and eight tephra layers have been identified (Figures 12 and 13; Table 3).

KC13 core ages range from present time to 250 ka (Figure 12). Sapropels S1 to S9 are observed and five tephra layers have been identified (Figures 12 and 13; Table 3).

KC15 core is truncated at the top. Ages range from 90 to 330 ka (Figure 4). Sapropels S6 to S10 are observed and four tephra layers have been identified (Figure s 12 and 13; Table 3).

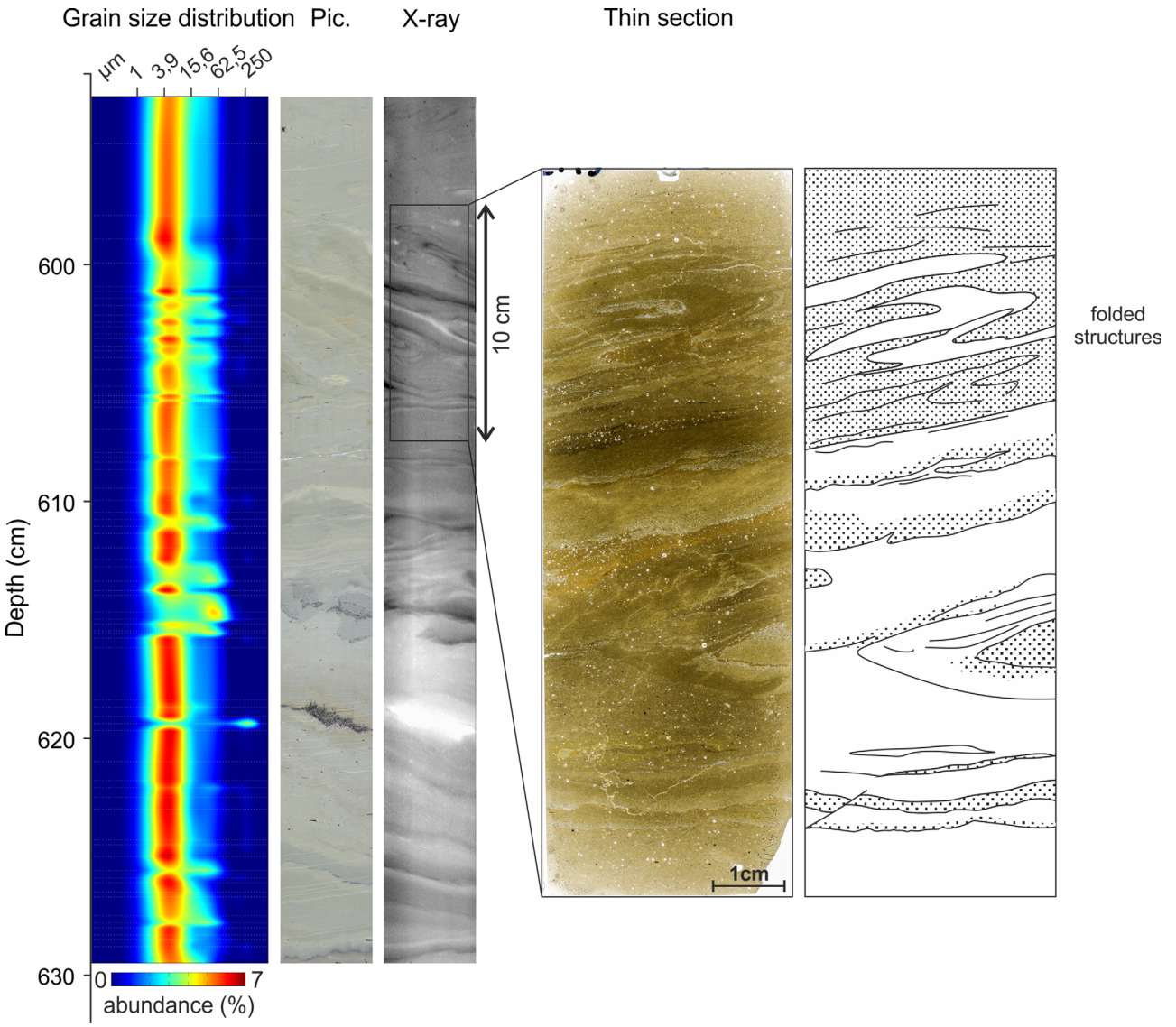

Figure 9. Grain size measurements, X-ray pictures and thin section of the folded and liquefaction facies present in core KC15. Grain size distribution is presented by cartography of the relative abundance of each fraction in percent (from dark blue for low abundance to dark red color for high abundance). Core location in Figure 1.

KC08 core ages range from present day to 320 ka (Figure 12). Sapropels S1, S3, S6, S7 and S9 are observed and three tephra layers have been identified (Figures 12 and 13; Table 3).

Geochemical oxide's values for all the cores are available in the supporting information.

6. Discussion

6.1. Stratigraphy

Tephra layers can be identified by comparing their composition with published data (Table 4 and Figure 13):

1. Tephra KC13-1 (28.8 ka) has the same composition as the Y3 eruption from Campanian province. Y3 was dated in literature at 30–31 ka (Zanchetta et al., 2008).
2. Tephra KC12-1 (30.3 ka) can be correlated by geochemical composition to the Codola eruption from Somma-Vesuvius dated in literature at 25.1 ka (Wulf et al., 2004).

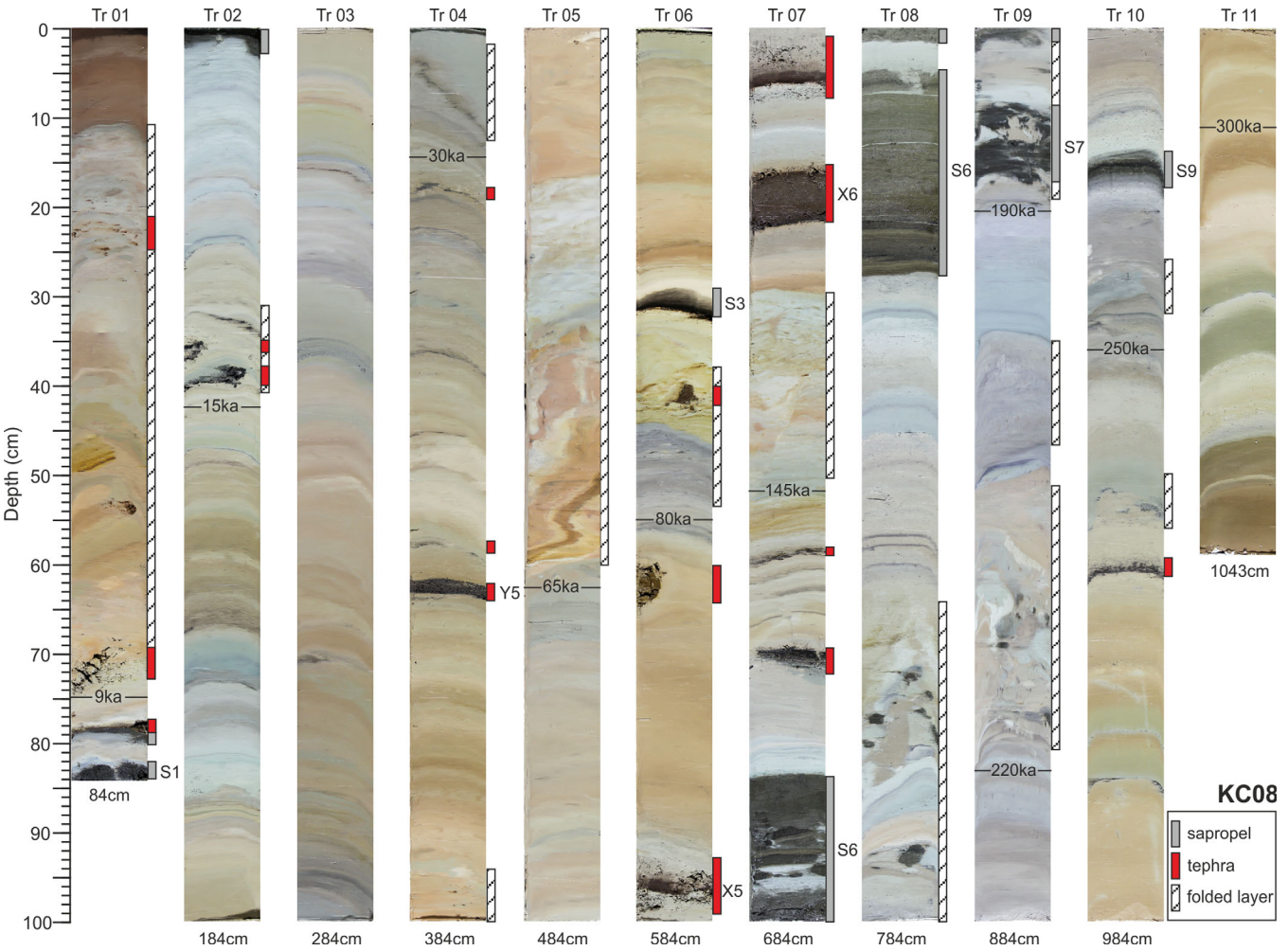

Figure 10. Picture of core KC08 with folded layers, tephra, sapropels and stratigraphic markers. Ages derives from the correlations with core KC07. Core location in Figure 1.

3. Tephra KC07-1 (38.1 ka), KC12-2 (37.8 ka), KC13-2 (38.4 ka) and KC08-1 (38.8 ka) can be correlated to the Y5 from Campanian province (Phlegrean Fields) dated in literature by $^{40}Ar/^{39}Ar$ geochronology at 39.28 $\pm$ 0.11 ka (De Vivo et al., 2001).
4. Tephra KC12-3 (43.9 ka) has the same composition as the Y6 eruption from Somma-Vesuvius. Y6 was dated in literature at 45 ka (Keller et al., 1978).
5. Tephra KC12-4 (103.7 ka), KC13-3 (103.4 ka), KC15-1 (97.6 ka) and KC08-2 (98 ka) can be correlated to the X5 from Campanian province. It is dated in literature by $^{40}Ar/^{39}Ar$ geochronology at 105 $\pm$ 2 ka (Allen et al., 1999; Kraml, 1998) and 106.2 $\pm$ 1.3 ka (Giaccio et al., 2012).
6. Tephra KC12-5 (106.7 ka), KC13-4 (107.6 ka), and KC08-3 (107.6 ka) have the same composition as the X6 from Campanian province dated in literature by $^{40}Ar/^{39}Ar$ geochronology at 108.9 $\pm$ 1.8 ka (Iorio et al., 2014).
7. Tephra KC12-6 (121.3 ka) and KC15-2 (124 ka) have the same composition as the C35/C36 from Campanian province dated in literature by Paterne et al. (2008) at 121.5 and 124 ka.
8. Tephra KC12-7 (127.9 ka) can be correlated to the P11 eruption from Pantelleria. It is dated by Paterne et al. (2008) at 130.6 ka.
9. Tephra KC12-8 (146.4 ka) has the same composition as the E24 eruption from Campanian province. It is dated by Paterne et al. (2008) at 148.4 ka.
10. Tephra KC13-5 (168.2 ka) can be correlated to the P12 eruption from Pantelleria. It is dated by Paterne et al. (2008) at 163.6 ka.

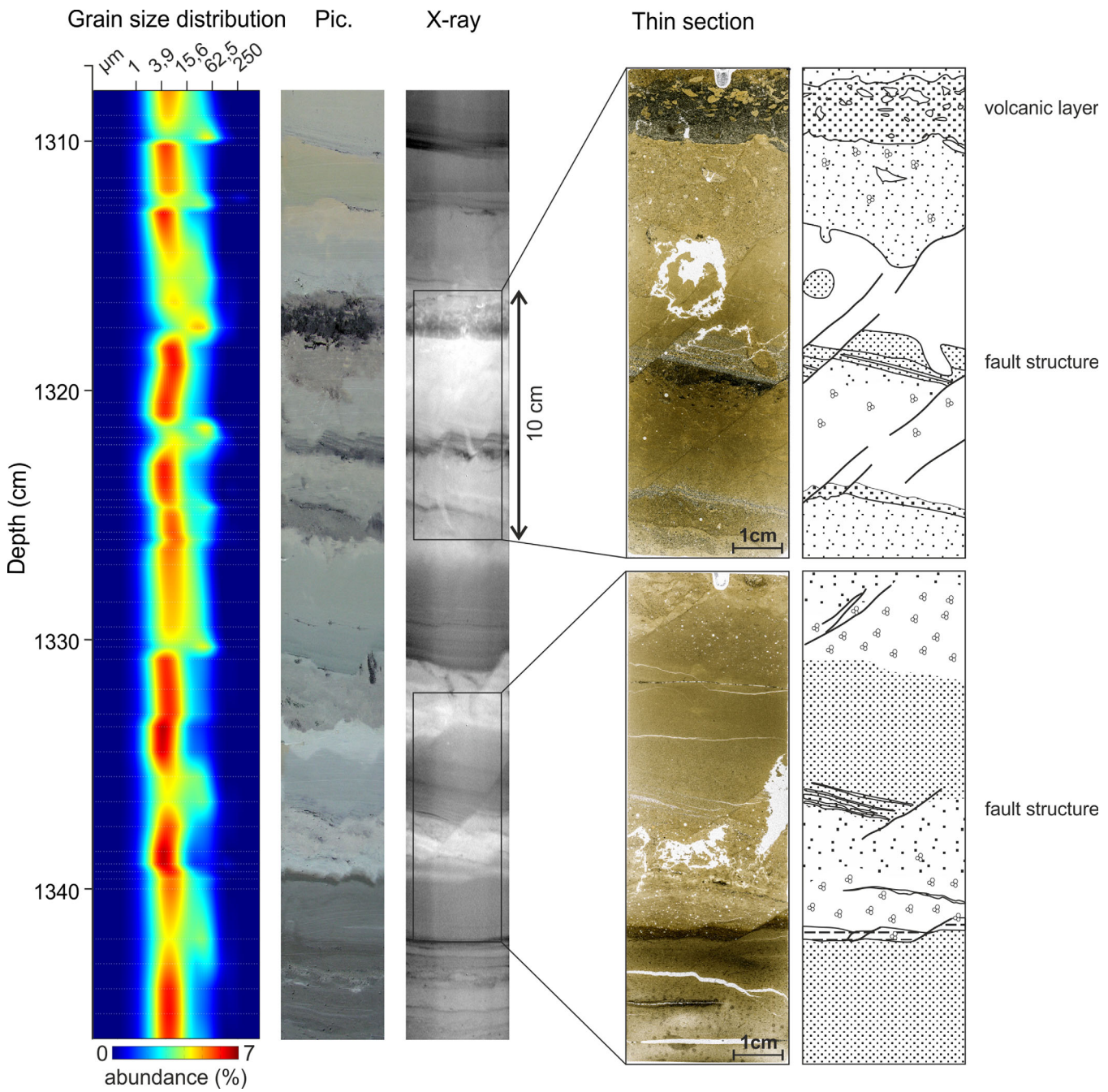

Figure 11. Grain size measurements, X-ray pictures and thin section of the fault facies present in core KC15. Grain size distribution is presented by cartography of the relative abundance of each fraction in percent (from dark blue for low abundance to dark red color for high abundance). Core location in Figure 1.

11. Tephra KC15-3 (249.2 ka) and KC15-4 (278.7 ka) have a similar composition than the Campanian province but no references have been found in literature.

Dating methods based on $\delta^{18}O$ correlations generate error margins linked to the measurement step, the sediment rates, error margin of the reference curve and the error due to the matching between curves. The differences between the tephra layer dating in our study and the ages provided in literature are inferior to 5 ka except in two cases. Although a remarkable difference around 8 ka can be noted in X5 layers in cores KC15 and KC08, this can be explained by the presence of folded layers that disturbed the dating. In the light of the time periods studied (300,000 years), this accuracy is quite acceptable to date the gravity-driven deposits recorded in the cores.

Table 2
Radiometric Ages for Samples Collected in Hemipelagic Sediments

Core	Core depth (cm)	Nature of sample	Radiocarbon age (BP)	Calibrated age (BP)
KC07	0	Planktonic foram.: *G. ruber*	2,960 ± 30	2,734 ± 25
	12	Planktonic foram.: *G. ruber*	5,015 ± 30	5,362 ± 48
	17	Planktonic foram.: *G. ruber*	6,665 ± 30	7,199 ± 35
	21	Planktonic foram.: *G. ruber*	8,000 ± 40	8,453 ± 49
	28	Planktonic foram.: *G. ruber*	9,815 ± 40	10,725 ± 73
	48	Planktonic foram.: *G. ruber*	14,465 ± 50	17,090 ± 105
	57	Planktonic foram.: *G. ruber*	18,040 ± 70	21,328 ± 141
	72–73	Planktonic foram.: *G. ruber*	25,180 ± 560	28,832 ± 607
	85–86	Planktonic foram.: *G. bulloides*	32,730 ± 260	36,205 ± 286
	93–94	Planktonic foram.: *G. ruber*	34,700 ± 1900	38,522 ± 2037

6.2. Frequency and Origin of the Gravity-Driven Deposits

6.2.1. Turbidites and Deformations

Processes responsible for generating gravity-driven deposits can be multiple: sea level changes, river discharges, storms, tsunamis, slidings or earthquakes. When gravity-driven deposits are triggered by sea level variability, the number of events increases during low sea level. This can be linked to an increase of continental surface and therefore to an increase of erosional processes (Stow et al., 1983) or during sea level fall or rise with slope destabilization (Shanmugam & Moiola, 1982). In this case, the changing sediment rates are significant. If we take the example of the Var system in the occidental basin of the Mediterranean Sea, sediment rates and turbidite frequency increase by a factor of 50 or more between the LGM and the Holocene (Bonneau et al., 2014).

Several studies have already been published on turbidite deposits on the Calabrian Arc. The first one (Kastens, 1984) studied debris flow and turbidite deposits emplaced between 17 and 10 ka on the post-Messinian ridge in the western lobe of the Calabrian Arc. Kastens (1984) deduces from these deposits return times between 1,000 and 3,000 years. Polonia et al. (2013b) studied three turbidite deposits recorded since AD1169 on the edge of the western Lobe and deduced a return time of around 500 years (CALA04, CALA05). Recently, Polonia et al. (2015) studied turbidite deposits recorded over the last 10 kyrs on pre-Messinian ridge on the eastern lobe (CALA21). They also deduced mean return times of around 500 years, although this varies between 100 and 700 years within the sapropel S1 deposit. The most recent study by Köng et al. (2016) highlights different return times depending on the

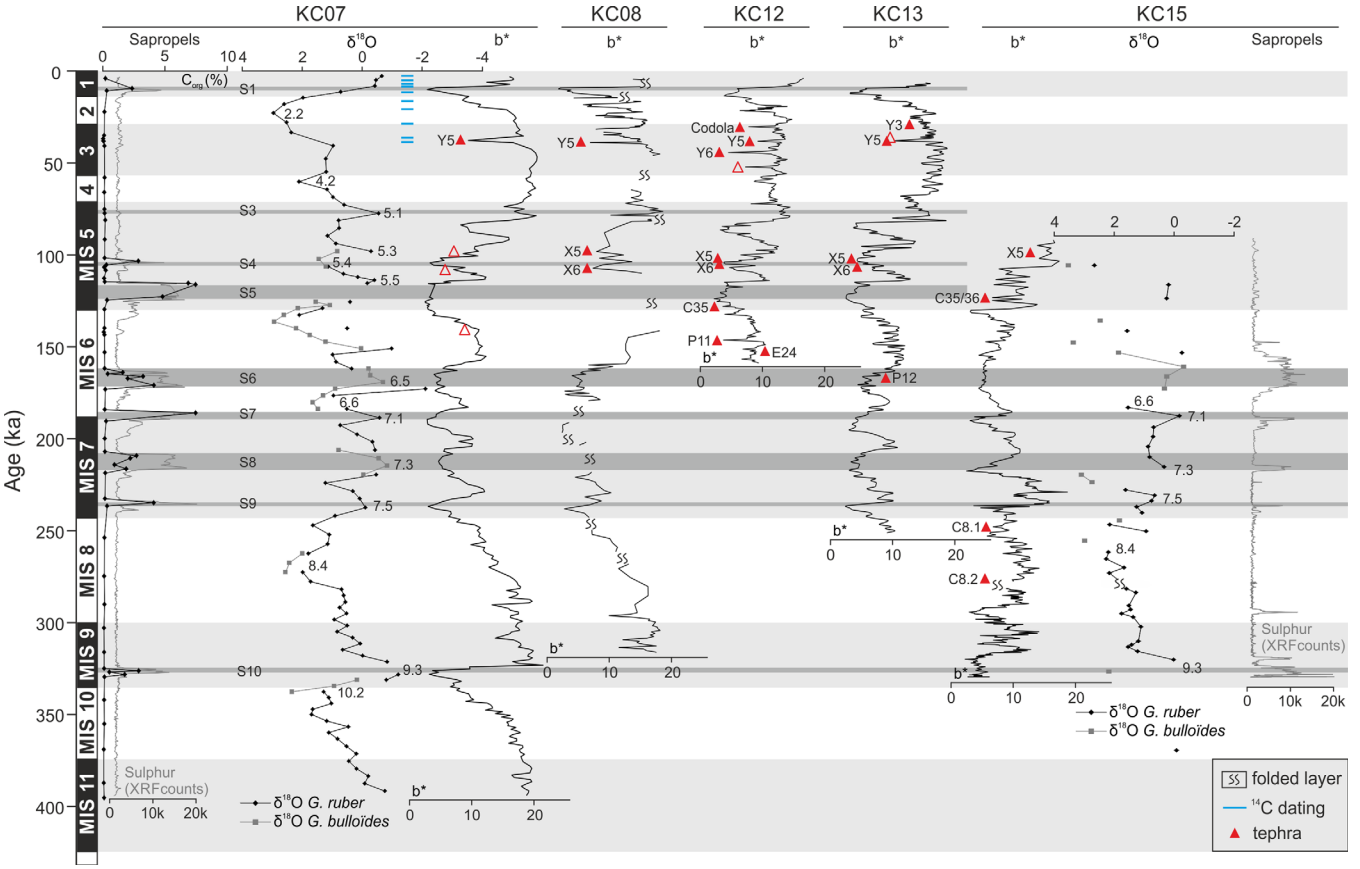

Figure 12. Stratigraphy based on δ18O, 14C and sapropels of core KC07 and correlations with KC08, KC12, KC13 and KC15 based on b* colour index curve. Blue lines correspond to radiocarbon dating of core KC07 (Table 2). Red triangles correspond to tephra layers and empty red triangle to not analyzed tephra layers.

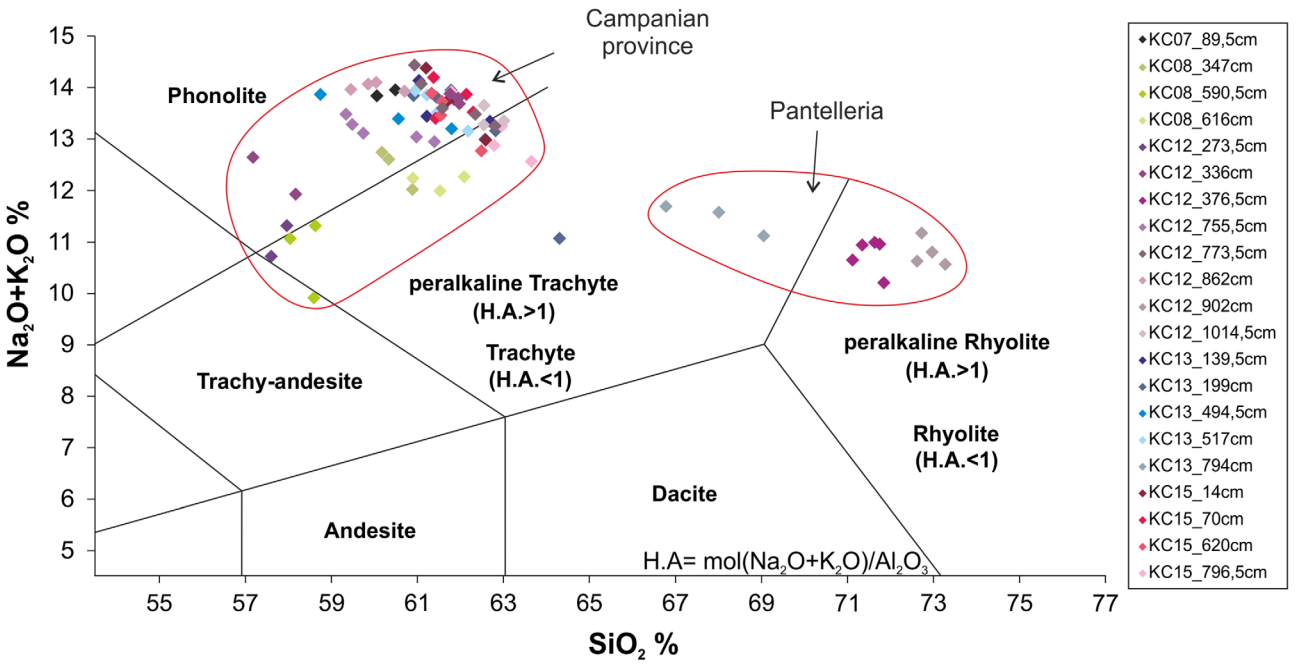

Figure 13. Total Alkali versus Silica (TAS – wt. %) diagram (Le Bas et al., 1986) classifies the glass shards as phonolitic, trachytic and rhyolitic populations in composition. H.A is the molecular ratio of the peralkaline index defined by H.A. = mol($Na_2O + K_2O$)/Al_2O_3. These compositional characters are compatible with Campanian and Pantelleria provenance. Geochemical oxide's values are available in the supporting information.

area in the western part of the Calabrian Arc over the last 60 kyrs: they vary between 450 and 1,000 years in the post-Messinian ridge (KC14) and are shorter in the Ionian abyssal plain (KC01) of around 240 years. On the Mediterranean Ridge, few studies are related to the turbidite activity on this accretionary wedge. Only one study in the Zakinthos and Strofadhes basins in the South of the Ionian Islands (Anastasakis & Piper, 1991) highlights return times between 125 and 450 years based on slumping layers during the deposition of sapropel S1.

Table 3
Tephra's Position, Thickness, Composition and Dating

Cores	Tephra layer	Depth (cm)	Thickness (cm)	Composition	Age obtained (ka)
KC07	KC07-1	89.5	5	Phonolite	38.1
KC12	KC12-1	273.5	3	Phonolite	30.3
	KC12-2	336	5.2	Phonolite	37.8
	KC12-3	376.5	4	Peralkaline-rhyolite	43.9
	KC12-4	755.5	11	Phonolite	103.7
	KC12-5	773.5	5	Phonolite	106.7
	KC12-6	862	0.2	Phonolite	121.3
	KC12-7	902	3	Peralkaline-rhyolite	127.9
	KC12-8	1014.5	8	Phonolite	146.4
KC13	KC13-1	139.5	1	Phonolite	28.8
	KC13-2	199	5	Trachy-phonolite	38.4
	KC13-3	494.5	1.2	Phonolite	103.4
	KC13-4	517	5.5	Phonolite	107.6
	KC13-5	794	3	Trachyte	168.2
KC15	KC15-1	14	1	Trachy-phonolite	97.6
	KC15-2	70	3	Trachy-phonolite	124
	KC15-3	620	1	Trachy-phonolite	249.2
	KC15-4	796.5	2.5	Trachy-phonolite	278.7
KC08	KC08-1	347	1.5	Trachy-phonolite	38.8
	KC08-2	590.5	1.5	Trachy-andesite	98
	KC08-3	606	6	Trachyte	107.6

The frequency of turbidites and deformations was calculated for each period of activity or non-activity recorded in the four studied cores. The duration of the interval is divided by the number of turbidites in order to obtain a median duration between recorded events. On the western Lobe of the Calabrian Arc, core KC15 appears to record two distinct periods of activity (Figure 16). The older, between 330 and 235 ka record an event every 990 years whereas the latest, between 235 and 90 ka record only 10 events, which corresponds to an event every 14,500 years. On the eastern lobe of the Calabrian Arc, core KC13 and core KC12 record two periods of activity (Figure 15). The older between 250 and 120 ka present return times of 14,000 years (KC12) and 3,900 years (KC13). The latest period between 120 and 12 ka records an event every 1,400 years (KC12 and KC13). On the western part of the Mediterranean Ridge, core KC08 appears to record two distinct periods of activity (Figure 15). The older, between 315 and 37 ka records on average an event every 10,000 years and the latest, between 37 ka and the present has return times of 1,000 years. These results highlights three periods of activity: a quiescent period between 235 and 125 ka surrounded by two more distinctive active periods (between 330 and 235 ka and between 125 ka to present) presenting a frequency of events of 1,000 years on average (Figure 16).

The upper part on the eastern lobe appears equally well supplied with return times twice as short as the deeper zones for the last 10 kyrs

Table 4
Dates of Tephra Obtained With Age Models Compared With Literature

		Age (ka)						Age in literature (ka)
Volcanic system	Eruption	KC07	KC12	KC13	KC15		KC08	Reference
Campanian	Y3			28.8			30–31	Zanchetta et al., (2008)
Somma-Vesuvius	Codola		30.3				25.1	Wulf et al. (2004)
Campanian	Y5	38.1	37.8	38.4		38.8	39.28 ± 0.11	De Vivo et al. (2001)
Somma-Vesuvius	Y6		43.9				45.0	Keller et al. (1978)
Campanian	X5		103.7	103.4	97.6	98	105 ± 2/106.2 ± 1.3	Allen et al. (1999); Kraml (1998); Giaccio et al. (2012)
Campanian	X6		106.7	107.6	106.7	107.6	108.9 ± 1.8	Iorio et al. (2014)
Campanian	C35/C36		121.3		124.0		121.5/124.0	Paterne et al. (2008)
Pantelleria	P11		127.9				130.6	Paterne et al. (2008)
Campanian	E24		146.4				148.4	Paterne et al. (2008)
Pantelleria	P12			168.2			163.6	Paterne et al. (2008)
Campanian	-				249.2/278.7		-	Unknown

(Polonia et al., 2015). Firstly, because of the presence of accretionary ridges that makes flowing across slope difficult. And furthermore, similar to the western part of the Calabrian Arc, because a trench has captured sediments from the Taranto Valley, the Calabrian Arc and the Apulia escarpment, allowing their transport directly from the continental shelf to the deepest zone along the Apulia escarpment (Figure 14). The central and external parts of the Calabrian Arc are starved in sediments and therefore record less turbiditic beds.

Contrary to the Calabrian Arc, the Mediterranean Ridge has no direct contact with the continental shelf. The presence of the Hellenic Trench to the East and of the Ionian abyssal plain to the West prevents direct sedimentary transit from the shelf to the ridge. The source of turbidites deposited in this area comes from more localized resedimentation process. As described by Moore and Karig (1976) on several accretionary wedges, vertical movements of accretionary ridges triggered destabilization of sediment already present on the

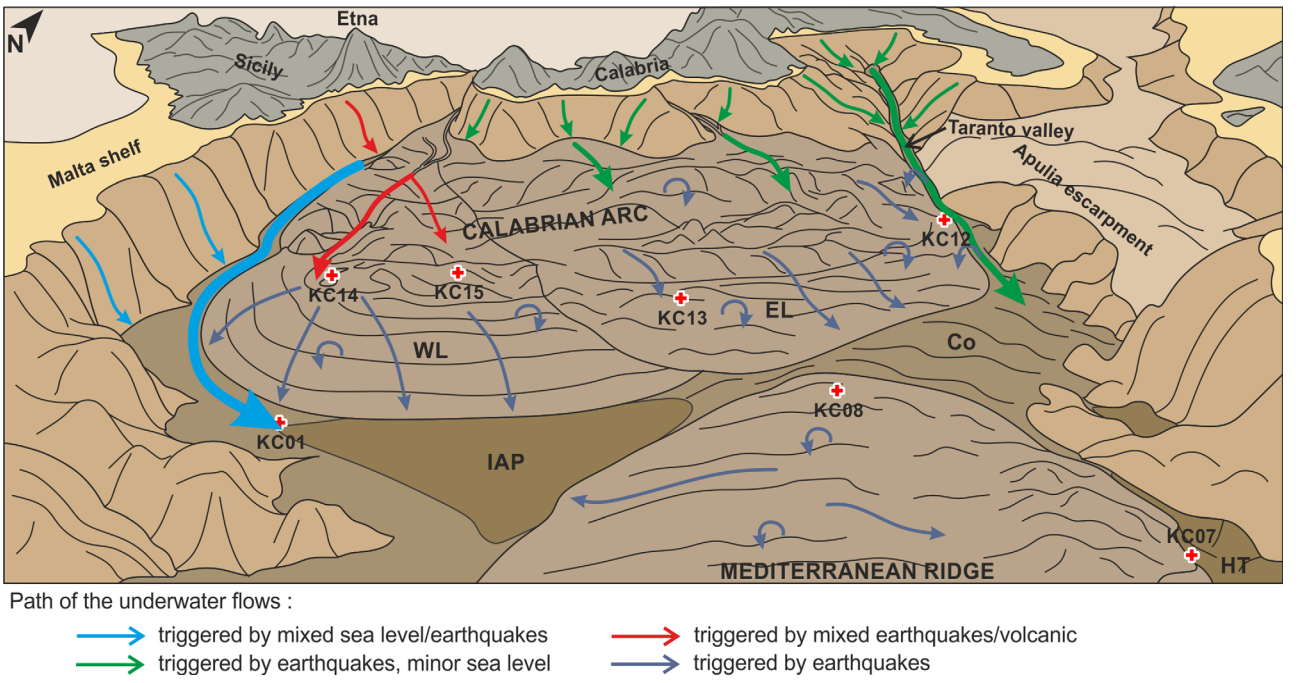

Figure 14. Reconstruction of the main underwater flows and their triggered on the Calabrian Arc and the western Mediterranean Ridge. Data for cores KC01 and KC14 derives from Köng et al. (2016). Acronyms correspond to: WL: Calabrian Arc western lobe, EL: Calabrian Arc eastern lobe, IAP: Ionian abyssal plain, Co: corridor between the Calabrian Arc and the Mediterranean Ridge, HT: Hellenic Trench.

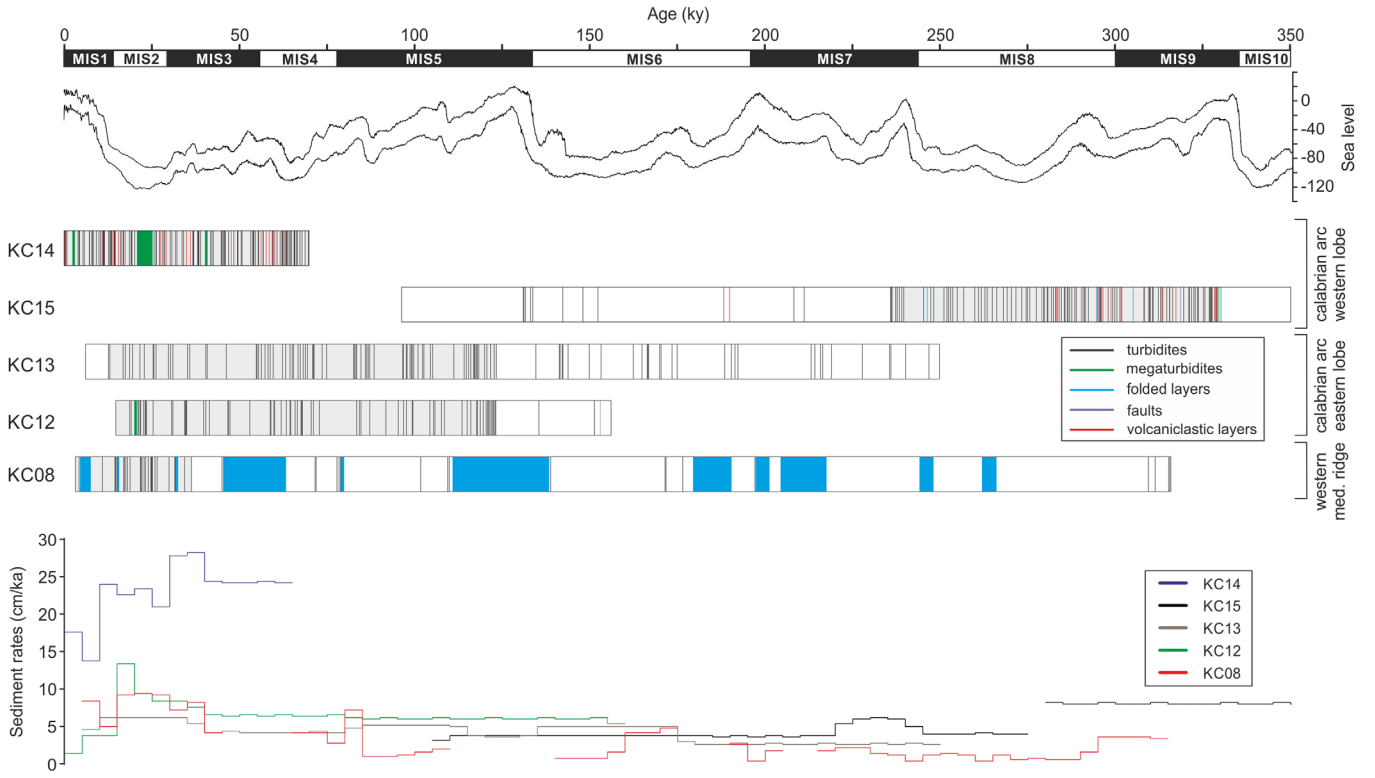

Figure 15. Log in age of the gravity-driven deposits (turbidites, megaturbidites, folded layers, faults and volcaniclastic layers). Data for cores KC01 and KC14 derived from Köng et al. (2016) and sea level curve from Grant et al. (2014). Acronym "IAP" corresponds to Ionian abyssal plain. Cores locations in Figures 1 and 12 for core KC14 and KC01.

ridge towards the slope basins (Figure 14). This phenomenon is probably applicable to the outer parts of the Calabrian Arc where sedimentary supplies from the Hellenic shelf are limited (Figure 14).

In the Ionian Sea, sediments rates appear to be relatively constant over the last 350 kyrs. The underdeveloped fluviatile systems in Sicily (watershed < 500 km^2) combined with an especially low level channelization on the Calabrian Arc which completely disappears below 2,000 m in depth (Köng et al., 2016) and the presence of two drainage axis between the Malta escarpement and the western lob of the Calabrian Arc and between the Apulia escarpement and the eastern lobe of the Calabrian Arc, strongly restricts sediment supply. On the Mediterranean Ridge, channelization is non-existent because the wedge is completely disconnected from the shelf by the Hellenic trench zone.

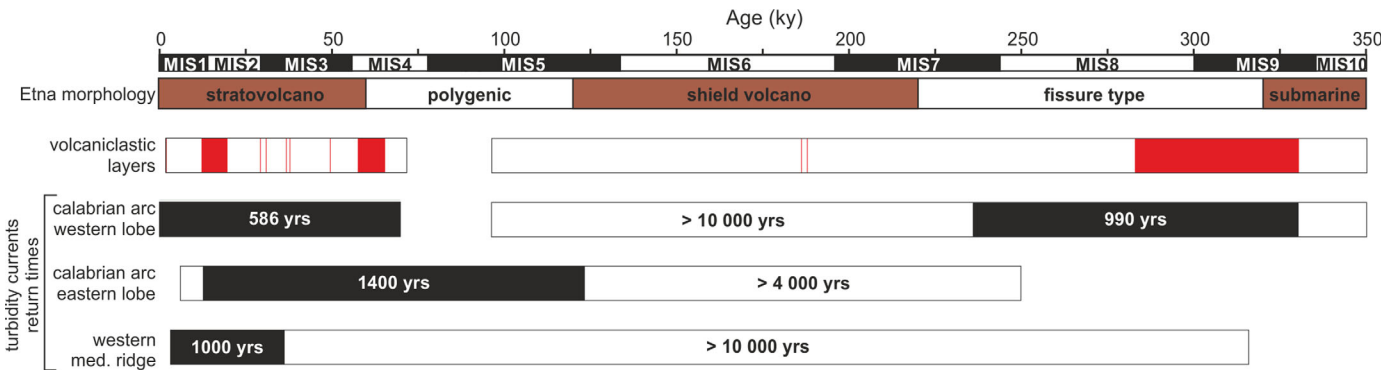

Figure 16. Overview of presence/absence periods of gravity-driven deposits of the accretionary wedges of the Ionian Sea and the occurrence of volcaniclastic layers linked to Etna morphology changing over the last 350 ka. Etna periods derives from Kieffer (1985) and Branca et al. (2008).

Previous studies on the Holocene showed that the gravity-driven deposits have a co-seismic origin (Polonia et al., 2013aa, 2013ab, 2015, 2016, 2017; San Pedro et al., 2017). The large majority of the seismo-turbidite deposits present amalgamated or stacked beds, characteristic of the deposition by multiple quasi-synchronous flows (Gutiérrez-Pastor et al., 2013; Migeon et al., 2017; Nelson et al., 2012; Polonia et al., 2016) and the presence of liquefaction figures and faults should be the witnesses of a co-seismic origin. Nevertheless, no palaeo-seismological studies have been reported for the older periods, it is therefore difficult to prove the co-seismic origin of sediment deposits at a several hundred of thousand years scale.

6.2.2. Megaturbidites

The basis of core KC15 is characterized by the deposit of four megaturbidites. The age model allows us to determine that these deposits are more than 300,000 years old. However, due to the composition of these megaturbidites and the lack of knowledge concerning this time scale, we are unable to clearly identify the origin of these four deposits.

The megaturbidite recorded in core KC12 is dated at around 21,000 years. This deposit is therefore contemporaneous of the two megaturbidites described by Köng et al. (2016) on the western lobe of the Calabrian Arc. As mentioned in this paper, the deposit is contemporaneous of the Cape-Riva caldeira of Santorini volcano which probably triggered a wide tsunami in the oriental Mediterranean Sea (Dominey-Howes & Minos-Minopoulos, 2004). However, the location of the deposit during low sea level may also be explained by the destabilization of methane hydrates on the continental shelf. This theory was already proposed by Reeder et al. (2000) and Rothwell et al. (2000) for megaturbidites found in the Levantine basin and in the occidental Mediterranean Sea dated around the same period.

6.2.3. Volcanoclastic Layers

On the western lobe of the Calabrian Arc, cores KC14 (Köng et al., 2016) and KC15 record two series of volcaniclastic layers (Figures 15 and 16). The older is situated between 330 and 280 ka and the latest between 60 ka and present day.

The Etna volcano is the nearest volcanic edifice of the study zone. Its morphology and magmatism has changed several times during the last 500 kyrs as its activity is closely linked to the surrounding tectonic activity (Branca et al., 2008; Kieffer, 1985).

The important instability recorded by turbidites in core KC15 is accompanied by the deposition of volcaniclastic layer with a trachytic composition (Figures 8 and 15). This could signify the expression of the fissural phase of the Etna (500 to 220 ka). The quiescent phase is contemporaneous with the shield volcano phase (220 to 120 ka) which seems to be linked to the extensional tectonic of the Timpe faults located in the south-east of Sicily, affecting the Ionian margin (Branca et al., 2008). The last phase observed in KC14 between 60 ka and present day is associated with the emplacement of volcanoclastic turbidites from the Etna (Figure 13; Köng et al., 2016). They could correspond to the building phase of the present-day stratovolcano.

7. Conclusion

In this study, the gravity-driven deposits recorded over the last 330 kyrs in the three different zones of the accretionary wedges (western and eastern lobe of the Calabrian Arc and the western part of the Mediterranean Ridge) highlight distinct periods of activity (Figure 16):

1. A period of activity between 330 and 225 ka in which gravity-driven deposits and volcanoclastic layers are recorded.
2. A quiescent period between 225 and 120 ka in which very few gravity-driven deposits are recorded.
3. A period of activity between 120 ka and present day in which gravity-driven deposits and volcanoclastic layers are recorded.

In addition, the presence of volcaniclastic layers derived from the western lobe of the Calabrian Arc suggest a record of Etna's morphological evolution since its emergence.

Acknowledgments
We would like to thank the SHOM (hydrological and oceanographic marine service) for the data, DGA (French Defence Procurement Agency, French Ministry of Defense) and CNRS (National Center of Scientific Research) of Normandy for PhD thesis funding, the 'ARTEMIS' technical platform for radiocarbon age dating. We are also grateful to EPOC technicians, engineers: P. Lebleu, I. Billy, B. Martin, O. Ther, B. Cosson, L. Rossignol and M.-H. Castera for the data acquisition. We thank J.-L. Devidal for his assistance with the electron microprobe. We would finally like to acknowledge Olivia Clayton and Lucia Hudson-Turner who provide English-language support and the three reviewers for their useful advices. Bathymetry, cores and sedimentological data are available from the French Hydrographic and Oceanographic Marine Service (SHOM; thierry.garlan@shom.fr).

References

Albert, P. G., Tomlinson, E. L., Lane, C. S., Wulf, S., Smith, V. C., Coltelli, M., . . . Menzies, M. A. (2013). Late glacial explosive activity on Mount Etna: Implications for proximal–distal tephra correlations and the synchronisation of Mediterranean archives. *Journal of Volcanology and Geothermal Research*, *265*, 9–26. https://doi.org/10.1016/j.jvolgeores.2013.07.010

Allen, J. R., Brandt, U., Brauer, A., Hubberten, H.-W., Huntley, B., Keller, J., . . . Negendank, J. F. (1999). Rapid environmental changes in southern Europe during the last glacial period. *Nature*, *400*(6746), 740–743.

Anastasakis, G. C., & Piper, D. J. W. (1991). The character of seismo-turbidites in the S-1 sapropel, Zakinthos and Strofadhes basins, Greece. *Sedimentology*, *38*(4), 717–733. https://doi.org/10.1111/j.1365-3091.1991.tb01016.x

Argnani, A. (2000). The Southern Tyrrhenian subduction system: Recent evolution and neotectonic implications. *Annals of Geophysics*, *43*.

Blaauw, M. (2010). Methods and code for "classical" age-modelling of radiocarbon sequences. *Quaternary Geochronology*, *5*(5), 512–518. https://doi.org/10.1016/j.quageo.2010.01.002

Blott, S. J., & Pye, K. (2001). GRADISTAT: A grain size distribution and statistics package for the analysis of unconsolidated sediments. *Earth Surface Processes and Landforms*, *26*(11), 1237–1248.

Bonneau, L., Jorry, S. J., Toucanne, S., Silva Jacinto, R., & Emmanuel, L. (2014). Millennial-scale response of a western Mediterranean River to late quaternary climate changes: A view from the deep sea. *The Journal of Geology*, *122*(6), 687–703. https://doi.org/10.1086/677844

Boyle, E., & Lea, D. (1989). Cd and Ba in planktonic foraminifera from the Eastern Mediterranean: Evidence for river outflow and enriched nutrients during sapropel formation. *Eos Transactions American Geophysical Union*, *70*, 1134.

Branca, S., Coltelli, M., De Beni, E., & Wijbrans, J. (2008). Geological evolution of Mount Etna volcano (Italy) from earliest products until the first central volcanism (between 500 and 100 ka ago) inferred from geochronological and stratigraphic data. *International Journal of Earth Sciences*, *97*(1), 135–152. https://doi.org/10.1007/s00531-006-0152-0

Çağatay, M. N., Wulf, S., Sancar, Ü., Özmaral, A., Vidal, L., Henry, P., . . . Gasperini, L. (2015). The tephra record from the Sea of Marmara for the last ca. 70 ka and its palaeoceanographic implications. *Marine Geology*, *361*, 96–110. https://doi.org/10.1016/j.margeo.2015.01.005

Calvert, S. (1983). Geochemistry of Pleistocene sapropels and associated sediments from the Eastern Mediterranean. *Oceanologica Acta*, *6*(3), 255–267.

Calvert, S., Nielsen, B., & Fontugne, M. (1992). Evidence from nitrogen isotope ratios for enhanced productivity during formation of eastern Mediterranean sapropels.

Calvo, J. P., Rodriguez-Pascua, M., Martin-Velazquez, S., Jimenez, S., & Vicente, G. D. (1998). Microdeformation of lacustrine laminite sequences from Late Miocene formations of SE Spain: An interpretation of loop bedding. *Sedimentology*, *45*(2), 279–292.

Catalano, S., & De Guidi, G. (2003). Late Quaternary uplift of northeastern Sicily: Relation with the active normal faulting deformation. *Journal of Geodynamics*, *36*(4), 445–467. https://doi.org/10.1016/S0264-3707(02)00035-2

Chapron, E., Beck, C., Pourchet, M., & Deconinck, J. (1999). 1822 earthquake-triggered homogenite in Lake Le Bourget (NW Alps). *Terra Nova*, *11*(2–3), 86–92.

Cita, M., & Grignani, D. (1982). Nature and origin of late neogene Mediterranean Sapropels, nature and origin of cretaceous carbon-rich fades SO Schlanger, MB Cita, 165–196.

Cita, M. B., & Aloisi, G. (1999). Deep-sea tsunami deposits triggered by the explosion of Santorini (3500 y BP), eastern Mediterranean. *Sedimentary Geology*, *135*(1–4), 181–203. https://doi.org/10.1016/S0037-0738(00)00071-3

Cita, M. B., Camerlenghi, A., & Rimoldi, B. (1996). Deep-sea tsunami deposits in the eastern Mediterranean: New evidence and depositional models. *Sedimentary Geology*, *104*(1–4), 155–173. https://doi.org/10.1016/0037-0738(95)00126-3

Cita, M. B., Vergnaud-Grazzini, C., Robert, C., Chamley, H., Ciaranfi, N., & D'onofrio, S. (1977). Paleoclimatic record of a long deep sea core from the eastern Mediterranean. *Quaternary Research*, *8*(2), 205–235. https://doi.org/10.1016/0033-5894(77)90046-1

Coy, F. M., Kastens, K., Gnaccolini, M., Giambastiani, M., Croce, M., Colombo, A., . . . Malinverno, A. (1983). Néotectonique des fonds sous-marins de la Dorsale Méditerranéenne en mer Ionienne au cours du Pléistocene moyen et supérieur. *Méditerranée*, 51–63.

D'Agostino, N., Avallone, A., Cheloni, D., D'anastasio, E., Mantenuto, S., & Selvaggi, G. (2008). Active tectonics of the Adriatic region from GPS and earthquake slip vectors. *Journal of Geophysical Research*, *113*, B12413, https://doi.org/10.1029/2008JB005860

Debret, M., Sebag, D., Desmet, M., Balsam, W., Copard, Y., Mourier, B., . . . Winiarski, T. (2011). Spectrocolorimetric interpretation of sedimentary dynamics: The new "Q7/4 diagram. *Earth-Science Reviews*, *109*(1–2), 1–19. https://doi.org/10.1016/j.earscirev.2011.07.002

De Lange, G. J., & Ten Haven, H. L. (1983). Recent sapropel formation in the eastern Mediterranean. *Nature*, *305*(5937), 797–798. https://doi.org/10.1038/305797a0

De Vivo, B., Rolandi, G., Gans, P., Calvert, A., Bohrson, W., Spera, F., & Belkin, H. (2001). New constraints on the pyroclastic eruptive history of the Campanian volcanic Plain (Italy). *Mineralogy and Petrology*, *73*(1–3), 47–65.

de Voogd, B., Truffert, C., Chamot-Rooke, N., Huchon, P., Lallemant, S., & Le Pichon, X. (1992). Two-ship deep seismic soundings in the basins of the Eastern Mediterranean Sea (Pasiphae cruise). *Geophysical Journal International*, *109*(3), 536–552.

Dewey, J., & Sengör, C. A. M. (1979). Aegean and surrounding regions: Complex multiplate and continuum tectonics in a convergent zone. *Geological Society of America Bulletin*, *90*(1), 84–92.

Dominey-Howes, D., & Minos-Minopoulos, D. (2004). Perceptions of hazard and risk on Santorini. *Journal of Volcanology and Geothermal Research*, *137*(4), 285–310. https://doi.org/10.1016/j.jvolgeores.2004.06.002

Dumas, B., Guérémy, P., & Raffy, J. (2005). Evidence for sea-level oscillations by the "characteristic thickness" of marine deposits from raised terraces of Southern Calabria (Italy). *Quaternary Science Reviews*, *24*(18), 2120–2136.

Emeis, K., Schulz, H., Struck, U., Rossignol, -Strick, M., Erlenkeuser, H., . . . Oba, T. (2003). Eastern Mediterranean surface water temperatures and δ18O composition during deposition of sapropels in the late Quaternary. *Paleoceanography*, *18*(1), 1005. https://doi.org/10.1029/2000PA000617

Emeis, K.-C., Sakamoto, T., Wehausen, R., & Brumsack, H.-J. (2004). The sapropel record of the eastern Mediterranean Sea—Results of Ocean Drilling Program Leg 160. *Palaeogeography, Palaeoclimatology, Palaeoecology*, *158*(3–4), 371–395. https://doi.org/10.1016/S0031-0182(00)00059-6

Emery, K., Heezen, B. C., & Allan, T. (1966). Bathymetry of the eastern Mediterranean Sea (Vol. 13, pp. 173–192). Presented at the Deep Sea Research and Oceanographic Abstracts, Elsevier.

Faccenna, C., Becker, T. W., Auer, L., Billi, A., Boschi, L., Brun, J. P., . . . Jolivet, L. (2014). Mantle dynamics in the Mediterranean. *Reviews of Geophysics*, *52*, 283–332. https://doi.org/10.1002/2013RG000444

Faccenna, C., Becker, T. W., Lucente, F. P., Jolivet, L., & Rossetti, F. (2001). History of subduction and back arc extension in the Central Mediterranean. *Geophysical Journal International*, *145*(3), 809–820.

Faccenna, C., Piromallo, C., Crespo, -Blanc, A., Jolivet, L., & Rossetti, F. (2004). Lateral slab deformation and the origin of the western Mediterranean arcs. *Tectonics*, *23*, TC1012. https://doi.org/10.1029/2002TC001488

Fountoulis, I., Mariolakos, I., & Ladas, I. (2014). Quaternary basin sedimentation and geodynamics in SW Peloponnese (Greece) and late stage uplift of Taygetos Mt. *Bollettino di Geofisica Teorica ed Applicata*, *55*, 303–324.

Gallais, F., Gutscher, M.-A., Graindorge, D., Chamot-Rooke, N., & Klaeschen, D. (2011). A Miocene tectonic inversion in the Ionian Sea (central Mediterranean): Evidence from multichannel seismic data. *Journal of Geophysical Research*, *116*, B12108. https://doi.org/10.1029/2011JB008505

Gallais, F., Gutscher, M.-A., Klaeschen, D., & Graindorge, D. (2012). Two-stage growth of the Calabrian accretionary wedge in the Ionian Sea (Central Mediterranean): Constraints from depth-migrated multichannel seismic data. *Marine Geology*, *326–328*, 28–45. https://doi.org/10.1016/j.margeo.2012.08.006

Giaccio, B., Nomade, S., Wulf, S., Isaia, R., Sottili, G., Cavuoto, G., . . . Sulpizio, R. (2012). The late MIS 5 Mediterranean tephra markers: a reappraisal from peninsular Italy terrestrial records. *Quaternary Science Reviews*, *56*, 31–45.

Goldfinger, C. (2011). Submarine paleoseismology based on turbidite records. *Annual Review of Marine Science*, *3*, 35–66.

Goldfinger, C., Grijalva, K., Bürgmann, R., Morey, A. E., Johnson, J. E., Nelson, C. H., . . . Chaytor, J. D. (2008). Late Holocene rupture of the northern San Andreas fault and possible stress linkage to the Cascadia subduction zone. *Bulletin of the Seismological Society of America*, *98*(2), 861–889.

Goldfinger, C., Nelson, C. H., & Johnson, J. E. (2003). Holocene earthquake records from the cascadia subduction zone and northern san andreas fault based on precise dating of offshore turbidites. *Annual Review of Earth and Planetary Sciences*, *31*(1), 555–577. https://doi.org/10.1146/annurev.earth.31.100901.141246

Goldfinger, C., Nelson, C. H., Morey, A. E., Johnson, J. E., Patton, J. R., Karabanov, E., . . . Dunhill, G. (2012). *Turbidite event history: Methods and implications for Holocene paleoseismicity of the Cascadia subduction zone*. Reston, VA: US Department of the Interior, US Geological Survey.

Grant, K., Rohling, E., Ramsey, C. B., Cheng, H., Edwards, R., Florindo, F., . . . Tamisiea, M. (2014). Sea-level variability over five glacial cycles. *Nature Communications*, *5*.

Gutiérrez-Pastor, J., Nelson, C. H., Goldfinger, C., & Escutia, C. (2013). Sedimentology of seismo-turbidites off the Cascadia and northern California active tectonic continental margins, northwest Pacific Ocean. *Marine Geology*, *336*, 99–119.

Gutscher, M.-A., Dominguez, S., de Lepinay, B. M., Pinheiro, L., Gallais, F., Babonneau, N., . . . Rovere, M. (2016). Tectonic expression of an active slab tear from high-resolution seismic and bathymetric data offshore Sicily (Ionian Sea). *Tectonics*, *35*, 39–54. https://doi.org/10.1002/2015TC003898

Hamann, Y., Wulf, S., Ersoy, O., Ehrmann, W., Aydar, E., & Schmiedl, G. (2010). First evidence of a distal early Holocene ash layer in Eastern Mediterranean deep-sea sediments derived from the Anatolian volcanic province. *Quaternary Research*, *73*(3), 497–506. https://doi.org/10.1016/j.yqres.2009.12.004

Hassoun, V., Martín, J., Migeon, S., Larroque, C., Cattaneo, A., Eriksson, M., . . . Levy, I. (2014). Searching for the record of historical earthquakes, floods and anthropogenic activities in the Var Sedimentary Ridge (NW Mediterranean). In *Submarine Mass Movements and Their Consequences* (pp. 571–581). Berlin, Germany: Springer.

Heezen, B. C., & Ewing, M. (1952). Turbidity currents and submarine slumps, and the 1929 Grand Banks earthquake. *American Journal of Science*, *250*(12), 849–873.

Huguen, C., Chamot-Rooke, N., Loubrieu, B., & Mascle, J. (2006). Morphology of a pre-collisional, salt-bearing, accretionary complex: The Mediterranean Ridge (Eastern Mediterranean). *Marine Geophysical Researches*, *27*(1), 61–75. https://doi.org/10.1007/s11001-005-5026-5

Huh, C., Su, C., Liang, W., & Ling, C. (2004). Linkages between turbidites in the southern Okinawa Trough and submarine earthquakes. *Geophysical Research Letters*, *31*, L12304. https://doi.org/10.1029/2004GL019731

Insinga, D. D., Tamburrino, S., Lirer, F., Vezzoli, L., Barra, M., De Lange, G. J., . . . Sprovieri, M. (2014). Tephrochronology of the astronomically-tuned KC01B deep-sea core, Ionian Sea: Insights into the explosive activity of the Central Mediterranean area during the last 200 ka. *Quaternary Science Reviews*, *85*, 63–84. https://doi.org/10.1016/j.quascirev.2013.11.019

Iorio, M., Liddicoat, J., Budillon, F., Incoronato, A., Coe, R. S., Insinga, D. D., . . . Tamburrino, S. (2014). Combined palaeomagnetic secular variation and petrophysical records to time-constrain geological and hazardous events: An example from the eastern Tyrrhenian Sea over the last 120 ka. *Global and Planetary Change*, *113*, 91–109. https://doi.org/10.1016/j.gloplacha.2013.11.005

Kastens, K. A. (1984). Earthquakes as a triggering mechanism for debris flows and turbidites on the Calabrian Ridge. *Marine Geology*, *55*(1–2), 13–33. https://doi.org/10.1016/0025-3227(84)90130-0

Kastens, K. A., & Cita, M. B. (1981). Tsunami-induced sediment transport in the abyssal Mediterranean Sea. *Geological Society of America Bulletin*, *92*(11), 845–857.

Keller, J., Ryan, W., Ninkovich, D., & Altherr, R. (1978). Explosive volcanic activity in the Mediterranean over the past 200,000 yr as recorded in deep-sea sediments. *Geological Society of America Bulletin*, *89*(4), 591–604.

Kieffer, G. (1985). *Evolution structurale et dynamique d'un grand volcan polygénique: Stades d'édification et activité actuelle de l'Etna(Sicile)* (Doctoral dissertation).

Köng, E., Zaragosi, S., Schneider, J.-L., Garlan, T., Bachèlery, P., San Pedro, L., . . . Racine, C. (2016). Untangling the complex origin of turbidite activity on the Calabrian Arc (Ionian Sea) over the last 60 ka. *Marine Geology*, *373*, 11–25. https://doi.org/10.1016/j.margeo.2015.12.010

Kraml, M. (1998). Laser-40 Ar, 39 Ar-Datierungen an distalen marinen Tephren des jung-quartären mediterranen Vulkanismus (Ionisches Meer, METEOR-Fahrt 25/4).

Kreemer, C., & Chamot-Rooke, N. (2004). Contemporary kinematics of the southern Aegean and the Mediterranean Ridge. *Geophysical Journal International*, *157*(3), 1377–1392.

Le Bas, M., Le Maitre, R., Streckeisen, A., & Zanettin, B. (1986). A chemical classification of volcanic rocks based on the total alkali-silica diagram. *Journal of Petrology*, *27*(3), 745–750.

Le Pichon, X., & Angelier, J. (1979). The Hellenic arc and trench system: A key to the neotectonic evolution of the eastern Mediterranean area. *Tectonophysics*, *60*(1–2), 1–42.

Le Pichon, X., Chamot-Rooke, N., Lallemant, S., Noomen, R., & Veis, G. (1995). Geodetic determination of the kinematics of central Greece with respect to Europe: Implications for eastern Mediterranean tectonics. *Journal of Geophysical Research*, *100*(B7), 12675–12690.

Lisiecki, L. E., & Raymo, M. E. (2005). A Pliocene-Pleistocene stack of 57 globally distributed benthic δ18O records. *Paleoceanography*, *20*, PA1003. https://doi.org/10.1029/2004PA001071

Lourens, L. J. (2004). Revised tuning of Ocean Drilling Program Site 964 and KC01B (Mediterranean) and implications for the δ18O, tephra, calcareous nannofossil, and geomagnetic reversal chronologies of the past 1.1 Myr. *Paleoceanography*, *19*, PA3010. https://doi.org/10.1029/2003PA000997

Löwemark, L., Lin, Y., Chen, H.-F., Yang, T.-N., Beier, C., Werner, F., . . . Kao, S.-J. (2006). Sapropel burn-down and ichnological response to late Quaternary sapropel formation in two$\sim$ 400 ky records from the eastern Mediterranean Sea. *Palaeogeography, Palaeoclimatology, Palaeoecology*, *239*(3), 406–425.

Marco, S., & Agnon, A. (1995). Prehistoric earthquake deformations near Masada, Dead Sea graben. *Geology*, *23*(8), 695–698. https://doi.org/10.1130/0091-7613(1995)023 $<$ 0695:PEDNMD$>$2.3.CO;2

McClusky, S., Balassanian, S., Barka, A., Demir, C., Ergintav, S., Georgiev, I., . . . Kahle, H. (2000). Global Positioning System constraints on plate kinematics and dynamics in the eastern Mediterranean and Caucasus. *Journal of Geophysical Research*, *105*(B3), 5695–5719.

McKenzie, D. (1978). Active tectonics of the Alpine—Himalayan belt: The Aegean Sea and surrounding regions. *Geophysical Journal International*, *55*(1), 217–254.
Migeon, S., Garibaldi, C., Ratzov, G., Schmidt, S., Collot, J.-Y., Zaragosi, S., & Texier, L. (2017). Earthquake-triggered deposits in the subduction trench of the north Ecuador/south Colombia margin and their implication for paleoseismology. *Marine Geology*, *384*, 47–62. https://doi.org/10.1016/j.margeo.2016.09.008
Migeon, S., Weber, O., Faugeres, J.-C., & Saint-Paul, J. (1999). SCOPIX: A new X-ray imaging system for core analysis. *Geo-Marine Letters*, *18*(3), 251–255.
Minelli, L., & Faccenna, C. (2010). Evolution of the Calabrian accretionary wedge (central Mediterranean). *Tectonics*, *29*, TC4004. https://doi.org/10.1029/2009TC002562
Moore, G. F., & Karig, D. E. (1976). Development of sedimentary basins on the lower trench slope. *Geology*, *4*(11), 693–697.
Mouslopoulou, V., Oncken, O., Hainzl, S., & Nicol, A. (2016). Uplift rate transients at subduction margins due to earthquake clustering. *Tectonics*, *35*, 2370–2384. https://doi.org/10.1002/2016TC004248
Murat, A. (1984). *Séquences et paléoenvironnements marins quaternaires: Une marge active: L'arc hellénique oriental* (Thèse de 3e cycle). Perpignan, France: Université de Perpignan.
Nakajima, T., & Kanai, Y. (2000). Sedimentary features of seismoturbidites triggered by the 1983 and older historical earthquakes in the eastern margin of the Japan Sea. *Sedimentary Geology*, *135*(1–4), 1–19. https://doi.org/10.1016/S0037-0738(00)00059-2
Negri, A., Capotondi, L., & Keller, J. (1999). Calcareous nannofossils, planktonic foraminifera and oxygen isotopes in the late Quaternary sapropels of the Ionian Sea. *Marine Geology*, *157*(1–2), 89–103. https://doi.org/10.1016/S0025-3227(98)00135-2
Nelson, C., Pastor, J. G., Goldfinger, C., & Escutia, C. (2012). Great earthquakes along the Western United States continental margin: Implications for hazards, stratigraphy and turbidite lithology. *Natural Hazards and Earth System Sciences*, *12*(11), 3191.
Noda, A., TuZino, T., Kanai, Y., Furukawa, R., & Uchida, J. (2008). Paleoseismicity along the southern Kuril Trench deduced from submarine-fan turbidites. *Marine Geology*, *254*(1–2), 73–90. https://doi.org/10.1016/j.margeo.2008.05.015
Óladóttir, B. A., Sigmarsson, O., Larsen, G., & Devidal, J.-L. (2011). Provenance of basaltic tephra from Vatnajökull subglacial volcanoes, Iceland, as determined by major-and trace-element analyses. *The Holocene*, *21*, 1037–1048.
Olausson, E. (1961). Studies of deep-sea cores. Sediment cores from the Mediterranean Sea and the Red Sea. *Reports of the Swedish Deep-Sea Expedition 1947–1948*, *8*, 335–391.
Olivet, J.-L., Bonnin, J., Beuzart, P., & Auzende, J.-M. (1982). Cinématique des plaques et paléogéographie: Une revue. *Bulletin de la Société géologique de France*, *7*, 875–892.
Owen, G. (1987). Deformation processes in unconsolidated sands. *Geological Society Special Publications*, *29*(1), 11–24.
Paillard, D., Labeyrie, L., & Yiou, P. (1996). Macintosh program performs time-series analysis. *Eos, Transactions American Geophysical Union*, *77*(39), 379–379.
Paterne, M., Guichard, F., Duplessy, J. C., Siani, G., Sulpizio, R., & Labeyrie, J. (2008). A 90,000–200,000 yrs marine tephra record of Italian volcanic activity in the Central Mediterranean Sea. *Journal of Volcanology and Geothermal Research*, *177*(1), 187–196. https://doi.org/10.1016/j.jvolgeores.2007.11.028
Patton, J. R., Goldfinger, C., Morey, A. E., Ikehara, K., Romsos, C., Stoner, J., . . . Vizcaino, A. (2015). A 6600 year earthquake history in the region of the 2004 Sumatra-Andaman subduction zone earthquake. *Geosphere*, *11*(6), 2067–2129.
Peccerillo, A. (2005). *Plio-quaternary volcanism in Italy*. Berlin, Germany: Springer.
Pedersen, T., & Calvert, S. (1990). Anoxia vs. productivity: What controls the formation of organic-carbon-rich sediments and sedimentary Rocks?(1). *AAPG Bulletin*, *74*(4), 454–466.
Polonia, A., Bonatti, E., Camerlenghi, A., Lucchi, R. G., Panieri, G., & Gasperini, L. (2013a). Mediterranean megaturbidite triggered by the AD 365 Crete earthquake and tsunami. *Scientific Reports*, *3*. http://doi.org/10.1038/srep01285
Polonia, A., Nelson, C. H., Romano, S., Vaiani, S. C., Colizza, E., Gasparotto, G., & Gasperini, L. (2017). A depositional model for seismoturbidites in confined basins based on Ionian Sea deposits. *Marine Geology*, *384*, 177–198. https://doi.org/10.1016/j.margeo.2016.05.010
Polonia, A., Panieri, G., Gasperini, L., Gasparotto, G., Bellucci, L. G., & Torelli, L. (2013b). Turbidite paleoseismology in the Calabrian Arc subduction complex (Ionian Sea). *Geochemistry, Geophysics, Geosystems*, *14*, 112–140. https://doi.org/10.1029/2012GC004402
Polonia, A., Romano, S., Çağatay, M. N., Capotondi, L., Gasparotto, G., Gasperini, L., . . . Torelli, L. (2015). Are repetitive slumpings during sapropel S1 related to paleo-earthquakes? *Marine Geology*, *361*, 41–52. https://doi.org/10.1016/j.margeo.2015.01.001
Polonia, A., Torelli, L., Mussoni, P., Gasperini, L., Artoni, A., & Klaeschen, D. (2011). The Calabrian Arc subduction complex in the Ionian Sea: Regional architecture, active deformation, and seismic hazard. *Tectonics*, *30*, TC5018. https://doi.org/10.1029/2010TC002821
Polonia, A., Vaiani, S. C., & de Lange, G. J. (2016). Did the AD 365 Crete earthquake/tsunami trigger synchronous giant turbidity currents in the Mediterranean Sea? *Geology*.
Pouderoux, H., Lamarche, G., & Proust, J.-N. (2012). Building an 18 000-year-long paleo-earthquake record from detailed deep-sea turbidite characterisation in Poverty Bay, New Zealand. *Natural Hazards and Earth System Sciences*, *12*, 2077–2101.
Pouderoux, H., Proust, J.-N., & Lamarche, G. (2014). Submarine paleoseismology of the northern Hikurangi subduction margin of New Zealand as deduced from Turbidite record since 16 ka. *Quaternary Science Reviews*, *84*, 116–131. https://doi.org/10.1016/j.quascirev.2013.11.015
Reeder, M. S., Rothwell, R. G., & Stow, D. A. V. (2000). Influence of sea level and basin physiography on emplacement of the late Pleistocene Herodotus Basin Megaturbidite, SE Mediterranean Sea. *Marine and Petroleum Geology*, *17*(2), 199–218. https://doi.org/10.1016/s0264-8172(99)00048-3
Reilinger, R., McClusky, S., Oral, M., King, R., Toksoz, M., Barka, A., . . . Sanli, I. (1997). Global Positioning System measurements of present-day crustal movements in the Arabia-Africa-Eurasia plate collision zone. *Journal of Geophysical Research*, *102*(B5), 9983–9999.
Reimer, P. J., Bard, E., Bayliss, A., Beck, J. W., Blackwell, P. G., Bronk Ramsey, C., . . . Friedrich, M. (2013). IntCal13 and Marine13 radiocarbon age calibration curves 0–50,000 years cal BP.
Reston, T., Fruehn, J., & von Huene, R. (2002). The structure and evolution of the western Mediterranean Ridge. *Marine Geology*, *186*(1–2), 83–110. https://doi.org/10.1016/S0025-3227(02)00174-3
Rodríguez-Pascua, M. A., Calvo, J. P., Vicente, D., G., &., & Gómez-Gras, D. (2000). Soft-sediment deformation structures interpreted as seismites in lacustrine sediments of the Prebetic Zone, SE Spain, and their potential use as indicators of earthquake magnitudes during the Late Miocene. *Sedimentary Geology*, *135*((1–4), 117–135. https://doi.org/10.1016/S0037-0738(00)00067-1
Rohling, E. J. (1994). Review and new aspects concerning the formation of eastern Mediterranean sapropels. *Marine Geology*, *122*(1–2), 1–28.
Rothwell, R. G., Reeder, M. S., Anastasakis, G., Stow, D. A. V., Thomson, J., & Kähler, G. (2000). Low sea-level stand emplacement of megaturbidites in the western and eastern Mediterranean Sea. *Sedimentary Geology*, *135*(1–4), 75–88. https://doi.org/https://doi.org/10.1016/S0037-0738(00)00064-6

Ryan, W. (1972). Stratigraphy of Late Quaternary sediments in the eastern Mediterranean. *The Mediterranean Sea*, *149*.
San Pedro, L., Babonneau, N., Gutscher, M.-A., & Cattaneo, A. (2017). Origin and chronology of the Augias deposit in the Ionian Sea (Central Mediterranean Sea), based on new regional sedimentological data. *Marine Geology*, *384*, 199–213. https://doi.org/10.1016/j.margeo.2016.05.005
Santoro, E., Ferranti, L., Burrato, P., Mazzella, M. E., & Monaco, C. (2013). Deformed Pleistocene marine terraces along the Ionian sea margin of southern Italy: Unveiling blind fault-related folds contribution to coastal uplift. *Tectonics*, *32*, 737–762, https://doi.org/10.1002/tect.20036
Shanmugam, G., & Moiola, R. (1982). Eustatic control of turbidites and winnowed turbidites. *Geology*, *10*(5), 231–235.
Siani, G., Paterne, M., Michel, E., Sulpizio, R., Sbrana, A., Arnold, M., & Haddad, G. (2001). Mediterranean Sea surface radiocarbon reservoir age changes since the last glacial maximum. *Science*, *294*(5548), 1917–1920.
Stow, D. A., Howell, D. G., & Nelson, C. H. (1983). Sedimentary, tectonic, and sea-level controls on submarine fan and slope-apron turbidite systems. *Geo-Marine Letters*, *3*(2–4), 57–64.
Thunell, R. C., Williams, D. F., & Kennett, J. P. (1977). Late Quaternary paleoclimatology, stratigraphy and sapropel history in eastern Mediterranean deep-sea sediments. *Marine Micropaleontology*, *2*, 371–388.
Tortorici, L., Monaco, C., Tansi, C., & Cocina, O. (1995). Recent and active tectonics in the Calabrian arc (Southern Italy). *Kinematics of Distributed Deformation in Plate Boundary Zones with Emphasis on the Mediterranean, Anatolia and Eastern Asia*, *243*(1–2), 37–55. https://doi.org/10.1016/0040-1951(94)00190-K
Truffert, C. (1992). De la compression de la Ride méditerranéenne à l'extension en mer Egée, Géodynamique de la Méditerranée orientale.
van Dijk, J. P., & Scheepers, P. J. J. (1995). Neotectonic rotations in the Calabrian Arc; implications for a Pliocene-Recent geodynamic scenario for the Central Mediterranean. *Earth-Science Reviews*, *39*(3–4), 207–246. https://doi.org/10.1016/0012-8252(95)00009-7
Van Os, B., Lourens, L., Hilgen, F., De Lange, G., & Beaufort, L. (1994). The formation of Pliocene sapropels and carbonate cycles in the Mediterranean: Diagenesis, dilution, and productivity. *Paleoceanography*, *9*(4), 601–617.
Vergnaud-Grazzini, C. (1985). Mediterranean late Cenozoic stable isotope record: Stratigraphic and paleoclimatic implications. In *Geological evolution of the Mediterranean Basin*. (pp. 413–451). Berlin, Germany: Springer.
Vergnaud-Grazzini, C., Ryan, W. B., & Cita, M. B. (1977). Stable isotopic fractionation, climate change and episodic stagnation in the eastern Mediterranean during the late Quaternary. *Marine Micropaleontology*, *2*, 353–370.
Viti, M., Mantovani, E., Babbucci, D., & Tamburelli, C. (2011). Plate kinematics and geodynamics in the Central Mediterranean. *Active Tectonics of the Circum-Adriatic Region*, *51*(2–3), 190–204. https://doi.org/10.1016/j.jog.2010.02.006
Völker, D., Scholz, F., & Geersen, J. (2011). Analysis of submarine landsliding in the rupture area of the 27 February 2010 Maule earthquake, Central Chile. *Marine Geology*, *288*(1), 79–89.
Wagner, B., Sulpizio, R., Zanchetta, G., Wulf, S., Wessels, M., Daut, G., & Nowaczyk, N. (2008). The last 40 ka tephrostratigraphic record of Lake Ohrid, Albania and Macedonia: A very distal archive for ash dispersal from Italian volcanoes. *Journal of Volcanology and Geothermal Research*, *177*(1), 71–80. https://doi.org/10.1016/j.jvolgeores.2007.08.018
Warning, B., & Brumsack, H.-J. (2000). Trace metal signatures of eastern Mediterranean sapropels. *Palaeogeography, Palaeoclimatology, Palaeoecology*, *158*(3), 293–309.
Wulf, S., Kraml, M., Brauer, A., Keller, J., & Negendank, J. F. W. (2004). Tephrochronology of the 100 ka lacustrine sediment record of Lago Grande di Monticchio (southern Italy). *Quaternary International*, *122*(1), 7–30. https://doi.org/10.1016/j.quaint.2004.01.028
Zanchetta, G., Sulpizio, R., Giaccio, B., Siani, G., Paterne, M., Wulf, S., & D'orazio, M. (2008). The Y-3 tephra: A Last Glacial stratigraphic marker for the central Mediterranean basin. *Journal of Volcanology and Geothermal Research*, *177*(1), 145–154. https://doi.org/10.1016/j.jvolgeores.2007.08.017
Zaragosi, S., Bourillet, J.-F., Eynaud, F., Toucanne, S., Denhard, B., Van Toer, A., & Lanfumey, V. (2006). The impact of the last European deglaciation on the deep-sea turbidite systems of the Celtic-Armorican margin (Bay of Biscay). *Geo-Marine Letters*, *26*(6), 317–329. https://doi.org/10.1007/s00367-006-0048-9
Zelilidis, A., Kontopoulos, N., Avramidis, P., & Piper, D. (1998). Tectonic and sedimentological evolution of the Pliocene–Quaternary basins of Zakynthos island, Greece: Case study of the transition from compressional to extensional tectonics. *Basin Research*, *10*(4), 393–408.